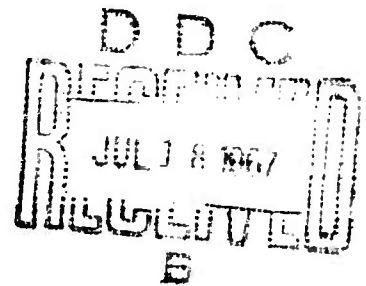# Glass Laser Damage Research

FINAL REPORT for
Office of Naval Research
Contract No. N 00014-66-C0159

JUNE, 1967

CORNING
CORNING GLASS WORKS

FINAL TECHNICAL REPORT

January, 1966 to June 30, 1967

Contract N00014-66-C0159

June 30, 1967

Glass Laser Damage Research

Corning Glass Works

Corning, New York

Order No. 306   Project Code No. 7300

Authors:

    R. D. Maurer

    W. W. Lester

    M. E. Vance

ABSTRACT

This report covers an experimental investigation into the damage of glass by high-intensity, 1.06μ wavelength light pulses of millisecond duration. Damage due to optical absorption by impurities is demonstrated by ease of damage, above some intrinsic level, proportional to the measured optical absorption. An additional source of damage is optical absorption at 1.06μ from the excited (fluorescing) state of the neodymium ion. Evidence for this mechanism is presented, and an approximate value of the excited state absorption cross section determined. The nonradiative decay (heating) back to the initial excited state is assumed to be the source of damage, and this appears reasonable from other data.

Studies of opto-acoustic coupling are presented and their connection with stimulated Brillouin scattering denoted. Measured coupling constants for different glasses, which are shown to be devoid of impurity optical absorption effects, are presented. Stimulated Brillouin scattering as a cause of damage suggests correlation between these opto-acoustic coupling constants and damage thresholds. Initial qualitative agreement between the two is encouraging enough to warrant further investigation of this technique as a way of predicting damage thresholds.

TABLE OF CONTENTS

1. INTRODUCTION

This final report covers a series of investigations into damage of glass by high-intensity light. Only internal fracture under millisecond pulses from a neodymium glass laser was studied. Many other problems such as surface pitting, solarization, etc., were omitted in order to concentrate on an area of concern that was more readily accessible to controlled experimentation and understanding. In addition, emphasis was placed on damage due to properties of the material itself rather than to stray inclusions. While damage due to inclusions certainly presents practical difficulties, the obvious solution is to eliminate the inclusions. Beyond this, more serious and intrinsic causes arise and these were thought to be of sufficient fundamental importance to glass laser design to warrant careful experimentation.

When inclusions are absent, a whole host of mechanisms have been postulated as possible damage causes. These include dielectric breakdown, two-photon absorption, stimulated Brillouin scattering, etc. All of them presumably lead to conversion of light into heat and consequent generation of large thermal expansion stress, although the stimulated Brillouin scattering could give large acoustic stresses as well. This report will deal with three mechanisms of damage - optical absorption by impurities in the glass, optical absorption by the excited state of neodymium in glass, and stimulated Brillouin scattering.

There are two basic reasons for studying the effect of absorp-
tion by impurities in glasses. First, this is a practical problem
since optical absorption due to impurities at levels common in
glass has been shown to lead to fracture.[1.1/] If host lattice
damage thresholds are raised by scientific investigation, the
purity must be similarly raised to keep pace. These impurities,
notably iron, have highly quenched decays from the excited state
but presumably some intensity level can be reached which will
saturate the transition, then impurity absorption damage thresholds
will stop rising with decrease in impurity level. This situation
has not yet been attained. Therefore the magnitude of the impurity
effects is presently an important design parameter. A second
reason for studying the effect of impurity absorption is to elimin-
ate it as a contributor in finding the intrinsic damage level.
Experimental values of the magnitude of the impurity absorption
effects is necessary if it is to be ruled out as a contributing
cause.

The reason for studying damage due to the neodymium ion is
obvious. If such a mechanism is operative, it is fruitless to
search for neodymium host lattices having unusually high damage
threshold since the addition of neodymium could immediately
reduce the threshold to a value commensurate with the effect of
neodymium in that lattice. An intrinsic limit may thus be present.
To our knowledge, this mechanism has not been previously proposed
and the object of the experiments was to obtain evidence on its

possibility as well as approximate values for the magnitude of the excited-state absorption. Some indications that the process is operable are given in this report.

Lastly, some experiments on optically generated acoustic waves are reported. These are an outgrowth of Company-funded research which was thought to have a bearing on the damage problem. The connection between these investigations and stimulated Brillouin scattering is superficially obvious. However, on closer inspection these experiments can only give part of the information necessary to understand damage by this mechanism. It was a desire to see how far this could be pushed which led to the present work. In particular, the possibility of a correlation between the electrostrictive constant (which couples the optical wave to the acoustic wave in the material) and damage threshold was sought. The experiments are not yet conclusive but results so far indicate that this is an avenue worthy of further exploration.

2. EFFECTS DUE TO OPTICAL ABSORPTION BY IMPURITIES

2.1 Theory of Stresses Arising from Optical Absorption

Almost all mechanisms for material damage imply the degradation of light power into heat and the subsequent generation of large thermal stresses from expansion differences. This is true of the impurity optical absorption discussed below. It is important to know whether such mechanisms are plausible. Unfortunately, it is not possible to calculate the stresses arising from these processes with any confidence because not enough is known about the temperature dependence of the material properties. However, as shown here, simple calculations suggest that sufficiently high stresses for fracture may arise.

In the experiments reported below, the unfocussed beam divergence and the angle of convergence of the focussed light beam are such that the maximum light intensity is concentrated in an approximately equi-dimensioned volume. Therefore, the heat deposition is considered to be inside a sphere. Heat conduction away from the volume is neglected. In time-dependent heat flow problems, temperatures rise over a characteristic distance $(Dt)^{\frac{1}{2}}$ from the heat source, where D is the thermal diffusivity and t the time. Therefore, neglecting heat flow away from the volume is equivalent to R >> $(Dt)^{\frac{1}{2}}$. This approximation is not well obeyed in the experiments. We then expect the calculated temperature rise to be higher than the experimental rise because of heat loss, and the calculated stress will be corres-

pondingly high as well. The thermal expansion will be considered
as constant. With increasing temperature, the thermal expansion
will rise and the calculated stress will be lower than the experi-
mental stress. This will help compensate for the heat flow
approximation. Little is known about the temperature dependence
of the other quantities in the calculation, although the specific
heat should increase somewhat with increasing temperature.

With these remarks, the temperature rise ΔT is given
approximately by

$$\Delta T = \frac{\alpha E_f}{c_v}$$

where E_f is the fracture energy flux, α the optical absorption
coefficient, and c_v the specific heat. The temperature rise gives
a volume change

$$\frac{\Delta V}{V} = \beta \Delta T$$

where β is the volumetric expansion coefficient. This then yields
a tangential tensile stress at the sphere surface of

$$S_f = \frac{2-\sigma}{3(1-\sigma)} \quad \frac{\beta E_f \alpha}{k \, c_v}$$

with k the volumetric compressibility. So that

$$E_f = \frac{3k \, c_v}{2\beta\alpha} \, S_f$$

Taking S_f to be the theoretical breaking strength of glass
(neglecting stress concentrating flaws) of 3×10^6 psi, and using the
expansion coefficient for liquid glass with typical values of
the other quantities for glass at 300°K, yields a fracture

threshold of about 3×10^5 joules cm^{-2} for an absorption
coefficient of 0.1 cm^{-1}. This is about the value observed
experimentally. However, as previously pointed out,[2.1] the
temperature changes of the various parameters are large and
the agreement is partly fortuitous. Nevertheless, the calcula-
tion shows that, with present information, we cannot neglect
absorption as a damage cause.

2.2 Fracture Thresholds for Optical Absorption by Impurities

It is clear from the previously developed theory that
if the dominant mechanism of damage by long pulses is optical
absorption, then the threshold energy density should be inversely
proportional to the optical absorption coefficient α at the laser
wavelength. This was found earlier to be qualitatively correct.[2.1,2.2]
To test this relationship and to examine the role of ferrous iron
in laser damage, we melted a series of iron-doped glasses having
(0.001-0.25 wt.%) Fe_2O_3 and α at 1.06µ in the range (0.002-0.6cm^{-1}).
These glasses were of a composition identical to that of Corning
Code 0580 laser glass except that the neodymium was omitted and
the batch materials were exceptionally pure. Great care was
taken to prevent contamination and to obtain high optical quality.
The resulting glasses had no striae but did have some small bubbles,
which had to be avoided in the damage experiments. Absorption
coefficients were determined with a Cary Model 14 Spectrophotometer,
using carefully cut and polished samples 7cm in length. Samples
for damage threshold determination were cut and polished and then

well annealed. The correlation between absorption coefficient α at 1.06 microns and weight per cent Fe_2O_3 dopant is portrayed in Figure 2.1. The Fe_2O_3 weight per cent doping is given by (0.25%) 2^{-m}, m = 0, 1, 2, ...9. The absorption coefficient is seen to follow the law $\alpha = (0.600 \text{ cm}^{-1}) 2^{-m}$ from m = 0 to m = 4. For higher m the additional absorption due to residual impurities (mostly ferrous iron) becomes noticeable. The undoped glass (sample J) and a control sample prepared from ultra-pure materials (sample L) fall at the low end of the curve and have $\alpha \approx 0.0025 \pm 0.0015 \text{cm}^{-1}$. Assuming a fixed ferrous-to-ferric iron ratio, this corresponds to a residual iron impurity of about 0.0008 weight per cent Fe_2O_3 plus 0.0003 weight per cent FeO.

2.2.1 Experimental Arrangement

Figure 2.2 shows the experimental arrangement for producing interior damage in the samples while simultaneously measuring the total energy, the spatial distribution, and the time variation of the laser beam before it reached the sample as well as the time variation of the intensity transmitted by the sample.

The laser was a 13-inch long by 1.5cm diameter Code 0580 neodymium glass rod with flat ends, completely immersed in a circulating K_2CrO_4-water coolant and placed between 99% and 30% external mirrors which were 86cm apart. The cloverleaf flashhead contained four EG&G FX-47-12 flashtubes each of which was in series with its individual 300-microhenry choke coil and

750-microfarad capacitor bank with 4KV power supply and series triggering circuit. At 3.5KV capacitor charge voltage, the laser output was nominally 35 joules with a pulse length of 1 millisec, a beam halfwidth of 0.8 millirad, and a spectral band width of 100Å at 1.06 microns. These values were reproducible to within a few per cent from shot to shot.

The far-field camera shown in the figure was as described in a previous report except that the 4-meter lens has been replaced by a 2-meter lens.[2.1] A series of far-field patterns stepped in intensity by a factor of 0.6 was recorded on the I-Z plate for a single laser shot. A reproduction of the I-Z plate for three such shots appears in Figure 2.3. The plate can thus be calibrated for each shot and microdensitometer tracings then allow a calculation of the relative energy distribution in the far field. Figure 2.4 shows a far-field profile (relative energy per unit solid angle versus angular displacement θ from direction of peak energy) taken through the center of the pattern for a 3.5KV shot.

The main beam was attenuated in small steps by means of suitable combinations of multiple-layer dielectric mirrors and uncoated plane-parallel flats, as indicated in Figure 2.2. Care was taken to see that reflected beams did not reenter the main beam. A portion of the attenuated beam was diverted to a photomultiplier and a calorimeter. The main beam was then focussed about 1cm deep into the sample by means of a

5cm focal length air-spaced doublet. Finally, a second photo-multiplier detected the 1.06 micron radiation transmitted by the sample. Both photomultiplier output voltages were observed by means of oscilloscope and camera. A sudden drop in the second photomultiplier output was taken as the beginning of fracture.

With the above arrangement, operating the laser at a fixed input voltage of 3.5KV, we obtained a repeatable far-field energy distribution and repeatable pulse shape. It was assumed that the far-field pattern varied in time in a repeatable manner. (Earlier measurements had shown an approximately linear growth of half-width with time.) The only variable was the amplitude of the pulse, which was proportional to the calorimeter output voltage. Under these conditions it could be assumed, in comparing two cases of fracture, that energy loss from the hot focal volume by conduction and radiation was the same, provided fracture occurred at the same time in each pulse. Thus the calorimeter output voltage was considered to be strictly proportional to the energy retained within the focal volume up to the instant of fracture and was therefore regarded as a valid measure of relative damage threshold energy. In the case of highly absorbing samples, a correction was necessary for the attenuation of the focussed beam within the sample before it reached the focus. Accordingly, the relative damage threshold E_D is proportional to (calorimeter voltage) x $e^{-\alpha D}$, where D is the depth of the focal spot within the sample.

2.2.2 <u>Results</u>

There is a surprisingly large variation of the
observed damage threshold in the same piece of glass. It is not
clear whether this was caused by variation in beam half-width time
dependence or by invisible inclusions in the sample. To get a
lower limit to the true damage threshold, the highest threshold
obtained for a given iron concentration was chosen. The recipro-
cals of these thresholds are plotted versus α in Figure 2.5 for
the four highest iron concentration glasses in the series. At
this point equipment difficulties forced us to postpone completion
of the series. Proceeding from the uppermost point in the figure,
one would expect the points to lie on a straight line through
the origin if optical absorption were the only mechanism involved.
If the optical absorption transition were to begin to saturate at
some low iron concentration, the curve would turn down toward the
α-axis. If a second damage mechanism were becoming important at
low concentrations, the curve would turn toward the E_D^{-1}-axis.
The limited data here indicate that optical absorption is the
dominant factor for large α (therefore low intensity) while a
second mechanism becomes dominant for small α (therefore high
intensity). If this second mechanism involves heating, we can
assume as a first approximation that the damageability E_D^{-1} is
given by the sum of two parts, one of which is proportional to α,
and the other of which is independent of α. That is, $E_D^{-1} = A\alpha + B$.
The linear fit to the data shown in Figure 2.5 then yields the

empirical relation

$$E_D = \frac{10^5 \text{ J/cm}^2}{(11.3\text{cm})\alpha + 1.0} \, .$$

The absolute energy thresholds used in getting this relation were obtained as follows. From the far-field energy distribution (Figure 2.4) we found that because of the circular symmetry only about 1/15 of the energy falls within the half-energy points of the one-dimensional profile. E_D is therefore computed as 1/15 of the total laser output energy divided by $\pi d^2/4$ where d is the distance between half-energy points computed for the 5cm focal length lens. The absolute magnitude of $E_D(\sim 10^5 \text{ J/cm}^2)$ may be high by perhaps a factor of 3 because of geometrical effects and loss of heat by conduction, while the corresponding intensity $(\sim 10^8 \text{ W/cm}^2)$ is probably a lower limit on the peak intensity sustained by the sample.

2.3 Elastic Pulse Generation by Optical Absorption

2.3.1 Introduction

It has been shown in Section 2.2 that a low optical absorption can cause glass to fracture in an intense laser beam due to the high temperatures and pressures generated in the glass. An additional cause of damage to glass in a laser beam may be stimulated Brillouin scattering, which comes about as an intrinsic property of glass independent of absorption. These two sources of damage in glass can both be studied by means of opto-acoustic coupling, that is, by observing the nature and amplitude of acoustic waves generated in glass on the passage of

a laser beam. In this Section, the elastic waves generated
in optically absorbing glasses will be treated. The intrinsic
opto-acoustic effect related to stimulated Brillouin scattering
is treated in Section 4. In order to separate these two effects
melts of glasses of various optical absorptions have been made,
and the results show the importance of considering the intrinsic
opto-acoustic effect in low-absorption glasses. In general, one
observes a curve of acoustic output versus absorption which has
a non-zero intercept for zero absorption. This suggests that
the damage threshold curve versus absorption should behave in a
similar way, showing an intrinsic damage threshold independent of
absorption.

When there is optical absorption in a glass, the
passage of a light beam will naturally heat the glass, and, in
the case of a pulsed laser beam, may contain enough energy to
heat the glass appreciably in a short time. If the glass has a
positive expansion coefficient, then the glass will expand from
thermal effects very rapidly, giving rise to a pressure jump in
the region illuminated by the laser beam. Assuming a circular
cross section for the laser beam, and normal incidence on a block
of glass with plane-parallel faces, the region illuminated will
be a cylinder. This cylinder will be heated by the laser beam,
giving rise to a pressure jump from the interior to the exterior
which is a function of the distance the laser beam has traveled
in the glass. This pressure jump gives rise to a longitudinal

wave directed radially outward from the cylinder; call this the radial wave. In addition, there will be a pressure gradient from one end of the cylinder to the other due to the laser beam being absorbed in the glass, which will give rise to an elastic wave traveling in the direction of the laser beam. Call this the longitudinal wave. There is yet a third wave generated due to the longitudinal wave having a boundary at the edge of the cylinder; this is a shear or transverse wave traveling radially outward. We will neglect this radial shear wave, as the experimental arrangement contemplated does not detect it.

2.3.2 Theory of Elastic Pulses Due to Optical Absorption

a. Assumptions

Assume that the incident laser beam is of circular cross section of radius r, and that it gives a single pulse whose effective duration is from time t_1 to time t_2. We will imagine that the laser beam strikes a block of glass, with plane parallel faces, normally with incident intensity $I_1(t)$. In order to simplify the calculation, assume that the elastic wave produced does not move an appreciable distance in the time the laser is on (t_2-t_1); that is, for practical purposes $r \gg C_o(t_2-t_1)$, where C_o is the velocity of longitudinal waves in the glass. This will facilitate calculating the total pressure jump from the interior to the exterior of the cylindrical region illuminated by the beam, but eliminates the details of the shape of the pressure jump from consideration. For example, if

$r = 1cm$, $t_2-t_1 = 10^{-7}sec$, $C_o = 5 \times 10^5 cm/sec$, then

$C_o(t_2-t_1) = .05cm \ll r$. We will also neglect the thermal

conductivity of and radiation from the medium.

Assume that the glass is uniform, its optical

absorption is constant and does not saturate, and that the

specific heat and thermal expansion coefficient are not

functions of the temperature.

b. The Radial Longitudinal Wave

Imagine an infinitesinal cube dxdydz located

inside the illuminated cylinder. The heat added to the cube dQ

in a temperature rise dT is

$$dQ = \rho \, C_v dT \, dxdydz, \qquad (1)$$

where ρ is the density and C_v the specific heat. (Since in

solids $C_p \approx C_v$, either will do here although neither is strictly

proper.)

So

$$\frac{dQ}{dx} = \rho \, C_v \, \frac{dT}{dX} \, dxdydz \qquad (2)$$

The laser beam is assumed to be directed along

the X axis, so the laser beam intensity I is related to dI/dx by

$$\frac{dI}{dx} = -\alpha I(x,t). \qquad (3)$$

Thus, the power W delivered to the cube is given by

$$\frac{dW}{dX} = \alpha I \, dydz, \qquad (4)$$

and

$$\frac{dQ}{dX} = dydz \, \alpha \int_{t_1}^{t_2} I dt. \qquad (5)$$

Inserting the value $I = I_1 e^{-\alpha x}$

$$\frac{dQ}{dx} = \alpha e^{-\alpha x}\, dydz \int_{t_1}^{t_2} I_1 dt. \tag{6}$$

Equating (2) and (6), we obtain

$$dT = \frac{\alpha e^{-\alpha x}}{\rho\, C_v} \int_{t_1}^{t_2} I_1 dt. \tag{7}$$

Now the thermal expansion coefficients α' is related to the volume change by

$$\frac{dV}{V} = \alpha' dT, \tag{8}$$

and

$$\frac{d\rho}{\rho} = -\frac{dV}{V}. \tag{9}$$

Noting that pressure P and ρ are related by the sound velocity for longitudinal waves in the material C_o, we have

$$\frac{dP}{d\rho} = C_o^2 = \frac{Y}{\rho}, \tag{10}$$

where Y is Young's modulus for the glass, and so

$$dP = C_o^2\, \rho\, \alpha' dT. \tag{11}$$

Using (7) we have the pressure jump as a function of X, the distance of travel in the block,

$$dP_{radial} = \frac{C_o^2\, \alpha\, \alpha' e^{-\alpha x}}{C_v} \int_{t_1}^{t_2} I_1 dt. \tag{12}$$

For example, assuming the laser energy density is $\int I_1 dt = 1$ joule/cm^2, $C_o = 5 \times 10^5$ cm/sec, $\alpha = 10^{-2}$ cm^{-1}, $C_v = .2$ cal/gm-deg, $\alpha' \sim 10^{-6}$, and noting that $\int I_1 dt$ must be measured in calories; (4.19 joules = 1 cal), we have at the entrance side of the block $X = 0$,

$$dP = 3 \times 10^3 \text{ dynes/cm}^2,$$

corresponding to a temperature jump of, for $\rho = 3\text{g/cm}^3$, $dT = 4 \times 10^{-3}$°C and a density change (condensation) of

$$\frac{d\rho}{\rho} = 4 \times 10^{-9}.$$

Noting that the product $\alpha \, \alpha'$ is proportional to dP, we see that for a heavily colored glass ($\alpha = 1$ cm^{-1}) of higher expansion $\alpha' = 10^{-5}$, one would obtain

$$\Delta P = 3 \times 10^6 \text{ dynes/cm}^2 = 3 \text{ atm,}$$

corresponding to a temperature jump of

$$\Delta T = .4°C$$

and a condensation of

$$\frac{d\rho}{\rho} = 4 \times 10^{-6}.$$

We thus note that, while the temperature changes are in general small (except for an opaque absorbing surface) and the density changes even smaller, quite respectable elastic waves may be generated in highly absorbing glasses using an ordinary unfocussed laser.

The elastic wave energy may be calculated approximately for the case of the 1 joule/cm^2 beam striking the

heavily colored glass ($\alpha = 1$ cm^{-1}), and yields

$$\int PdV = C_o^2 \rho \alpha'^2 V \int_{300°}^{300.4°} (T-300°)d(T-300°) \qquad (13)$$

$$\approx 1.2 \times 10^{-6} \text{ joules/cm}^3.$$

We then see that in a 1 cm^3 volume, only $\sim 10^{-6}$ part of the laser energy appears as an elastic wave. (The kinetic energy of the wave has been neglected, but is expected to be of the same order as the potential energy given above). We therefore draw the conclusion that, for the case of laser beams falling on a typical glass, the energy carried away by the elastic wave produced is in general a very small fraction of the laser energy if thermal expansion is the mechanism involved.

c.   The Longitudinal (longitudinal) Wave

The longitudinal wave generated in the direction of travel of the laser beam represents a pressure jump from entrance to exit face of

$$dP(x=0) - dP(x=\ell) = \frac{C_o^2 \alpha' \alpha}{C_v} \left(1-e^{-\alpha \ell}\right) \int_{t_1}^{t_2} I_1 dt, \qquad (14)$$

proportional to the absorption of the block $(1-e^{-\alpha \ell})$.

The local gradient is just

$$\frac{d}{dx}(dp) = \frac{-C_o^2 \alpha' \alpha^2}{C_v} e^{-\alpha x} \int_{t_1}^{t_2} I_1 dt. \qquad (15)$$

For small α glasses, or more properly small $\alpha \ell$ products, we have the total pressure drop approximately given by

$$dP_{long} = dP(x=0) - dP(x=\ell) = \frac{C_o^2 \alpha' \alpha^2 \ell}{C_v} \int_{t_1}^{t_2} I_1 dt. \qquad (16)$$

The radial pressure drop under these circumstances would be, at the entrance face,

$$dP_{radial} = \frac{C_o^2 \, \alpha \, \alpha'}{C_v} \int_{t_1}^{t_2} I_1 dt, \qquad (17)$$

larger by a factor $1/\alpha'$. Thus for the glass considered in section c, $\alpha = .01$, let $' = 1cm$, and the longitudinal component can be neglected in comparison with the radial. In the limit that α' becomes large, the longitudinal and radial pressure drops become comparable.

d. Measurement Technique

It is proposed to measure the elastic wave produced by means of an ultrasonic longitudinal wave transducer bonded to the glass block. The transducer yields a voltage proportional to the total force acting on its face in a fast pulse. In the event that the transducer length is as large as, or larger than, the block thickness $'$, the relative transducer response to be expected from otherwise-similar blocks having different α-values is given by the relative magnitude of the total force acting on the surface of the illuminated cylinder,[*]

$$\int_A P dA = \frac{2\pi r \, C_o^2 \, \alpha'}{C_v} \int_{t_1}^{t_2} I_1 dt (e^{-\alpha'} - 1) + \frac{\sigma \pi r^2 \, C_c^2 \alpha'}{C_v} \int_{t_1}^{t_2} I_1 dt (\alpha)(e^{-\alpha'} - 1), \quad (18)$$

---

[*] The reason the total force is calculable so nicely is that the pressure falls off as $1/r$, but $\int P dA$ does not fall off except due to absorption. In an experiment where a constant fraction of solid angle is subtended by the transducer, the calculation relates pressures in different blocks.

(σ being Poisson's ratio) the first term being due to the radial,
and the second, the longitudinal wave's effect at right angles to
its direction of propagation.

It is seen that the effect of the longitudinal
wave is smaller by the factor $\frac{\sigma r \alpha}{2}$, and thus is often very small
and can be neglected. Furthermore, for the case of small αl, the
terms in Eq. 17 become linear in the block thickness l, and the
acoustic wave appears to be generated uniformly in the volume
of the medium. This can be a useful approximation in relating
the transducer voltages obtained in blocks of different sizes.

2.3.3 Experimental Investigation

a. Apparatus

A block diagram of the experimental apparatus
for investigating the elastic waves from laser irradiated glasses
is shown in Fig. 2.6. The usual arrangement of dielectric mirrors,
laser rod and dye cell was set up to produce bleachable dye
Q-switched pulses from the exit mirror which then strike the glass
block. The back and front mirrors have reflectances of 99% and
85%, respectively, at 1.06μ. The laser beam energy is detected,
after passing through the glass block, by the photodiode (an
Edgerton, Germeshausen and Grier Lite Mike Model 560) diffusing
screen-filter combination. The diffusing screen was found
necessary to eliminate the effects of the filamentary nature of
the laser beam from causing false readings at the small photodiode
aperture. The transducer is a nominal 266KHz barium titanate
transducer for longitudinal waves bonded to the glass with

stopcock grease; its output is amplified (by three Hewlett-Packard Model 460A wide band amplifiers) and displayed side by side with the integrated laser energy on a dual beam oscilloscope (Tektronix Model 555). The laser supply (a TRG Model 106 with a Model 106-2 flashhead) is pumped at 7,200 joules with a bleachable dye (Eastman Q-Switch Solution #9740) absorbance of .35 to yield single pulses of $\leq$.5 joule at the glass block. The laser rod is a 1.5 x 15cm cylinder of Corning Code 0580 neodymium doped laser glass which emits at 1.06μ.

b. Measurement Technique

In operation, the oscilloscope is set with a delayed sweep of several hundred μsec, triggered by the pumping trigger pulse. It is not known to better than several hundred μsec, when the laser will Q-switch. This arrangement allows a faster sweep speed to be used. Then the oscilloscope is set on delayed single-sweep operation, and the traces are photographed as the laser is fired. Typical traces at a sweep speed of 100 μsec/cm for both are shown in Figs. 2.7-2.8. Here Fig. 2.7, the upper oscilloscope photograph shows the acoustic pulse (lower trace) resulting from a Q-switched laser pulse (integrated energy in upper trace) in 843KS[1], a low-absorption lead glass. The lower photograph (Fig. 2.8) shows the acoustic pulse (lower trace) resulting from Q-switched laser pulse (upper trace) in 843KS, an identical lead glass except for the addition of traces of nickel to produce large absorption at 1.06μ. The vertical scales in

Figs. 2.7 and 2.8 are not the same; 843KS produces ~25 times
as large   an acoustic signal for the same light energy as
843KS[1]. We note the very striking change of the character of
the acoustic output as the absorption is increased, namely, the
shift to predominance of low-frequency components in the trans-
ducer output as is seen for example by decrease damping of the
acoustic wave. This change takes place gradually as the optical
absorption is increased, and is connected with the intrinsic
ability of the glass to produce elastic waves in this experimental
situation independent of optical absorption; this will be treated
in detail in Section 4.

The transducer, a 1" square 266KHZ barium titanate
ceramic poled for longitudinal waves, responds to the net
compression or rarefaction integrated over the face area and
existing in its thickness at any time. That is, for example,
an elastic pulse step function traversing the transducer yields
a triangular output repetitive at the ringing frequency as the
resultant. The transducer responds less to higher-frequency
components accordingly as a whole number of wavelengths contained
in the transducer will cancel themselves in the voltage output.
The sensitivity of the transducer in terms of open circuit
voltage per unit applied step function of force such as is pre-
sent due to the action of the laser beam has been treated by
Redwood[2.3] and is found to be

$$V = \frac{-2h\ P\,!}{q(Z_t + Z_g)} \qquad\qquad (19)$$

where the voltage V is generated in the first quarter cycle of transducer oscillation, h is the piezoelectric constant of the transducer material, P the applied pulse pressure assumed uniform over the face, l the transducer thickness, C_t the velocity of longitudinal waves in the transducer, and Z_t and Z_g are the specific acoustic impedances of the transducer and glass, respectively. Inserting the values for the particular transducer at hand (furnished by Gulton Industries) results in the value $V = 1.46 \times 10^{-3}$ P, where V is in volts and P in dynes/cm^2, if one assumes $Z_t = Z_g$. The assumption that $Z_t = Z_g$ is rarely if ever exactly correct; Eq. (19) takes into account the reflection of the elastic waves from the glass-transducer boundary, which are absent if the acoustic impedances Z_t and Z_g are equal. An additional consideration arises in the circumstance that the piece of glass bonded to the transducer happens to have a resonance or antiresonance at one of the transducer resonance frequencies (2n+1) 266KHZ or antiresonances (2n) 266KHZ, where n is an integer. In this case, the coupled system will produce a spurious voltage increase (resonance-resonance) or decrease (antiresonance-resonance or antiresonance-antiresonance) from the calculated sensitivity due to the ringing, or lack of ringing as the case may be, in the block beyond the first quarter cycle. For this reason, the longitudinal wave velocities in all the glasses considered for opto-acoustic interaction work have been measured, using pulse techniques at 3.43MHZ, and the final glass blocks cut in cubes of a size not frequency sensitive near 266KHZ.

c. Experimental Results In Specific Glasses

In order to investigate in detail the dependence of the laser-induced elastic pulse amplitude on laser energy and absorption coefficient, a series of colored glasses were melted, and cut and polished samples prepared. One such series of glasses, the 843KS series, consisted of a lead-based glass of index 1.59 with successively higher absorptions produced by introducing trace amounts of nickel oxide in the melt. One-inch cubes of this glass were prepared.

Another series of glasses, the 95EV series, consistes of the base laser glass (index of refraction 1.53) for Corning Code 0580 lasers with the neodymium doping removed, and traces of iron (always present as an impurity) added to produce various absorptions at 1.06 microns. Eighteen-mm cubes of this glass were prepared for use.

Yet a third series, the 825E series consisted of melts colored with various metallic ions. In this series the blocks were not prepared as cubes, but were arbitrarily cut and polished into rectangular parallelpipeds $\frac{1}{2}$ x 1-1/16 x 2 inches. The laser beam was passed normally through the $\frac{1}{2}$-inch thickness with the transducer bonded to the 1-1/16 x 2 inch face.

Data was taken in each glass of each series by observing the peak to which the voltage signal from the transducer (proportional to P) rises versus the integrated light energy $E = \int_{o}^{t} Idt$ as measured by the photodiode. Only single-

pulse laser shots were considered. The absorption of each sample was determined in a Cary Recording Spectrophotometer at 1.06μ in order to obtain α and the value of $A = 1-e^{-\alpha l}$ for use in data plotting. In obtaining the data, six to ten laser shots were typically fired and the value P/E determined for each glass, typical statistical probable errors of 3% to 5% being obtained in the value of P/E. P was found proportional to E over a range of E typically from 1:5 in each glass, as Q-switched pulses vary in E from shot to shot, thus verifying one aspect of the theory. Data plots of the values of P/E obtained in the iron-doped laser glasses 95EV versus A (small absorption) and versus A (large absorption) are shown in Figs. 2.9 and 2.10, respectively. The theory predicts, in the absence of any other effect, the proportionality of P/E to A in the region of interest. We note however that when experimental data are taken, one finds an intercept on the ordinate showing that there remains some intrinsic pressure per unit light energy P/E for the case of negligable absorption (see glass EVL in Fig. 2.9). The discussion and measurement of such intrinsic effects is given in Section 4 of this report.

Other than this intrinsic intercept, the data shows the proportionality of P/E to A in Fig. 2.9 predicted by Eq. (18), for small α. In the case of larger α (see Fig. 210) there is some curvature in the data, which overlaps the region of Fig. 2.9, but no large anomalies, and there is general agreement with the theory for α somewhat larger than in Fig. 2.9.

A typical glass was chosen from the laser glass series, and numerical calculations made to see whether absolute agreement could be obtained between the theoretical result, Eq. (12), and the data. The gain of the amplifying system connected to the transducer was found by applying pulse-modulated signals to the input terminals from a low-impedance source at 266KHZ. The measured transducer voltages were then converted to pressures by means of Eq. (19), making use of the value of specific acoustic impedance Z_t = 28.7 x 10^6M.K.S. units and Z_g = 14.9 x 10^6 M.K.S. units. The resulting calibration for the ordinates of Figs. 2.9 and 2.10 shows that the numerical values of P/E in the glass can be obtained by multiplying the value read off the ordinate by 16.5 dynes/joule, or 16.5 dynes/cm^2/ joules/cm^2. In a specific glass cube, 95EVV, (see Fig. 2.10) the pressure amplitude per unit light energy is found to be P/E = 43.8 dynes/joule. The mean pressure across the face of the transducer calculated from Eq. (12) and the known values of the physical constants for this glass is P/E = 148.3 dynes/joule, larger than the measured value. The agreement is not bad, considering a number of sources of error which will be discussed later. Also, one takes note of the fact that the curve in Fig. 2.10 drops at large values of A, resulting in a somewhat too small value compared with other glasses lower on the curve such as 95EVQ. The slope of the straight-line portion of Fig. 2.9 is of special interest, since the values of P/E for

all the lower-lying glasses EVN-EVS can be predicted from it.
The slope measured from the data graph is found to be 125 dynes/joule,
while the theoretical value from Eq. (12) is 164 dynes/joule, in
good agreement with the measured value. Once again, the measured
value is lower than the theoretical one.

The data for the case of the nickel-doped lead
glass (the 843KS series) is shown in Figs. 2.11 and 2.12. The
calibration for the ordinates of these data graphs has been
calculated using Eq. (19), with the values Z_t = 28.7 x 10^6MKS
units and Z_g = 16.4 x 10^6MKS units. The result is that the ordinate
values may be multiplied by 5.26 dynes/joule in order to obtain
absolute values of P/E in the glass. This calculation takes
account of the reflected elastic wave from the glass-transducer
boundary. One sees, taking into account the calibrations in the
cases of the 95EV-series and the 843KS series, that the intrinsic
effect (ordinate intercept) is larger for the higher-index glass
(843KS). Fig. 2.11 shows a gentle curvature of P/E vs A,
suggesting that the large intrinsic effect is masking the pro-
portionality to A expected of P/E at low α. For large α, one
may neglect the first term of Eq. (18) and keep the second,
giving a proportionality between P/E and αA. This is demonstrated
by Fig. 2.12, where the data of Fig. 6 has been replotted for the
lead glass, showing the predicted proportionality. One thing
that is left unexplained is the value of α at which one should
use the second term of Eq. (18) and neglect the first. The two

terms bear the ratio $\sigma r \alpha/2$, and $r \sim 1$, $\sigma \sim .2-.3$ in most glasses, so one would expect $\alpha \sim 3$ to 5 cm^{-1} to be the region where the second term begins to become important. Instead, $\alpha \leq .4 cm^{-1}$ for the nickel-doped lead glasses, so quantitatively one should never see the second term at all.

The third series of glasses, the 825E-series yielded graphs of P/E versus A and αA (Figs. 2.13 and 2.14, respectively) which look more nearly ideal than the previous two glasses. This may be due to the fact that this glass has a very small intrinsic output not explained by Eq. (18) (see the intercept on Fig. 2.13). The predicted proportionality of P/E to A is seen for small α, and the proportionality to αA is seen for large α. As the largest α, for glass ER, is only .6, the transition from the use of the first term of Eq. (18) to the second term is still unexplained. The calibration of the ordinate is obtained easily, as for this glass $Z_t = Z_g = 28.7 \times 10^6$ MKS units within the experimental error; the ordinate values, multiplied by 8.28 dynes/joule, give the absolute values of P/E in the glass.

d. Sources of Error

It should be noted that, in the calculations of absolute magnitudes of elastic pulse pressure amplitude per unit light energy P/E, and in the slope of the curve of P/E versus $A = 1 - e^{-\alpha l}$, experimental values smaller than the theoretical ones

were obtained. This can be due to a number of causes. First
of all, the open-circuit sensitivity of the transducer was
calculated, whereas in the actual experiment a fairly low input
impedance amplifier was used which would lower the transducer
voltage somewhat. In addition, the spreading of the cylindrical
elastic wave in traversing the glass block before reaching the
transducer was neglected; this would cause the pressure
amplitude to fall off as r/r_o, where r_o is the radius of the laser
beam. It should be noted that r_o, has been assumed equal to the
radius of the laser rod, which is not strictly true. Finally,
the curvature of the cylindrical wavefront of the elastic wave
on arrival at the transducer face was neglected, which would
result in a measured low value. In view of these sources of
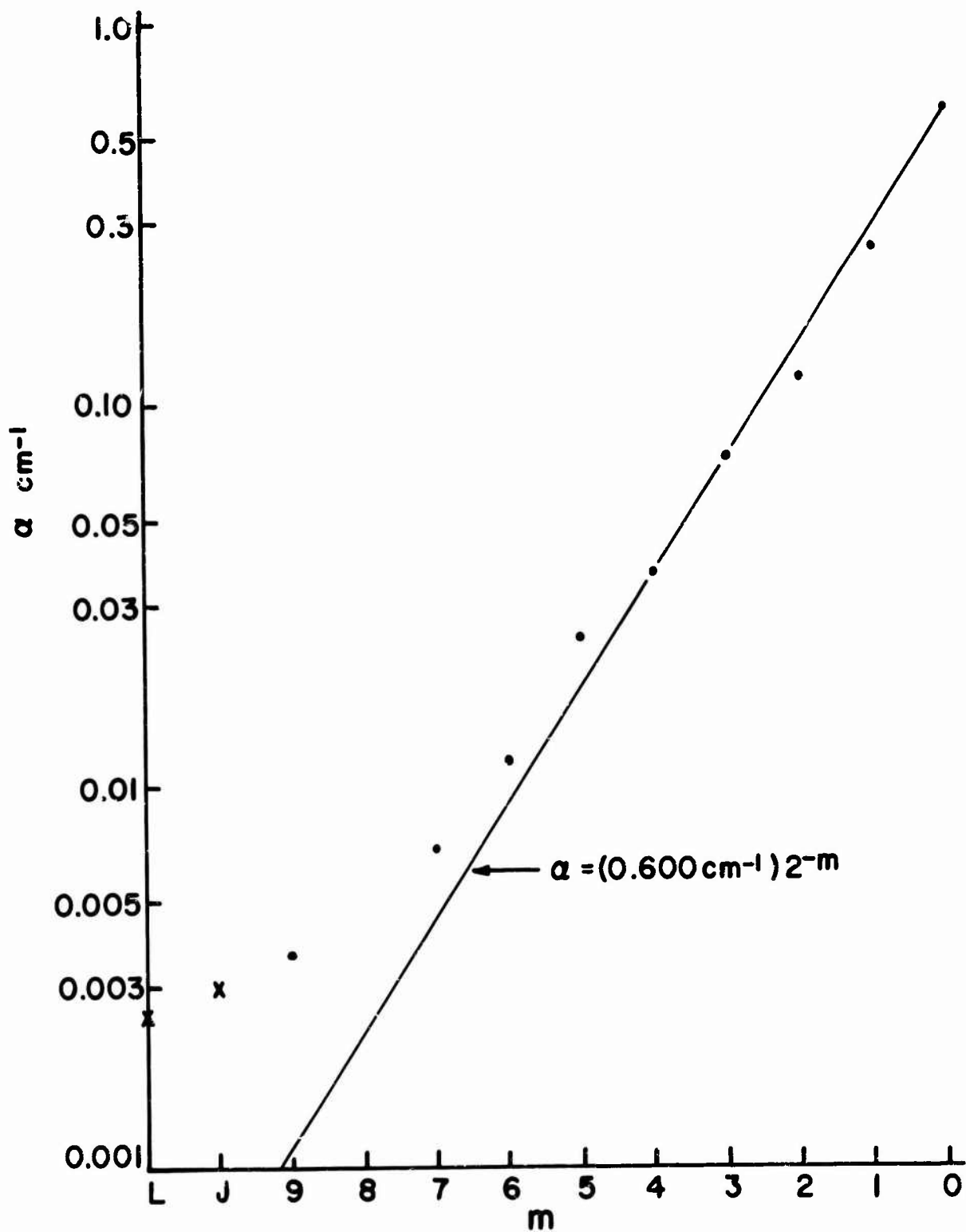error, the agreement between theory and experiment may be considered
good.

Fig. 2.1 Correlation of Measured Absorption Coefficients With
Weight Per Cent Fe_2O_3 Dopant. Solid Line is Theoretical,
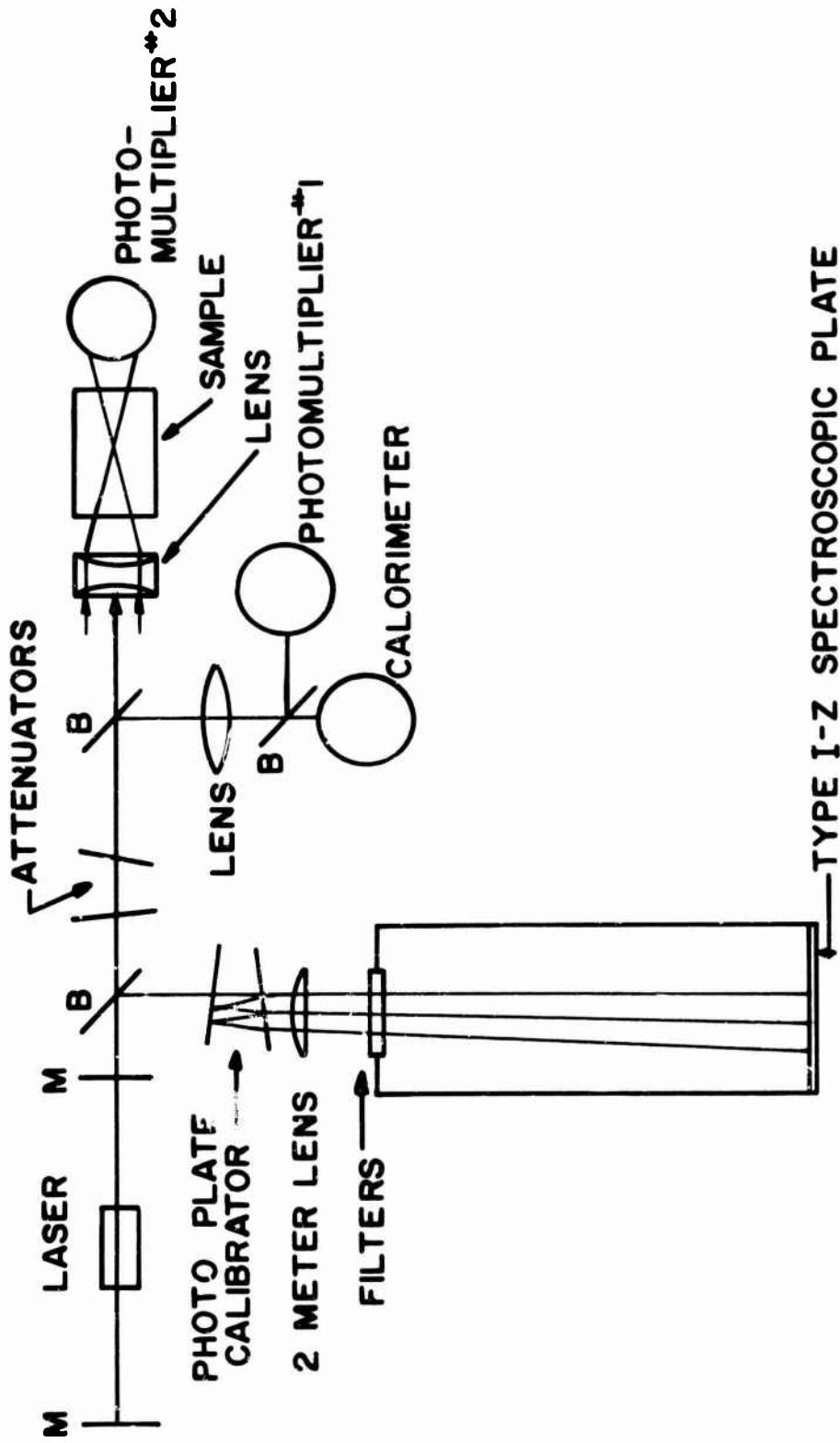Points are experimental for Doped Glasses, x's for undoped.

Fig. 2.2 Experimental Arrangement for Determining Damage
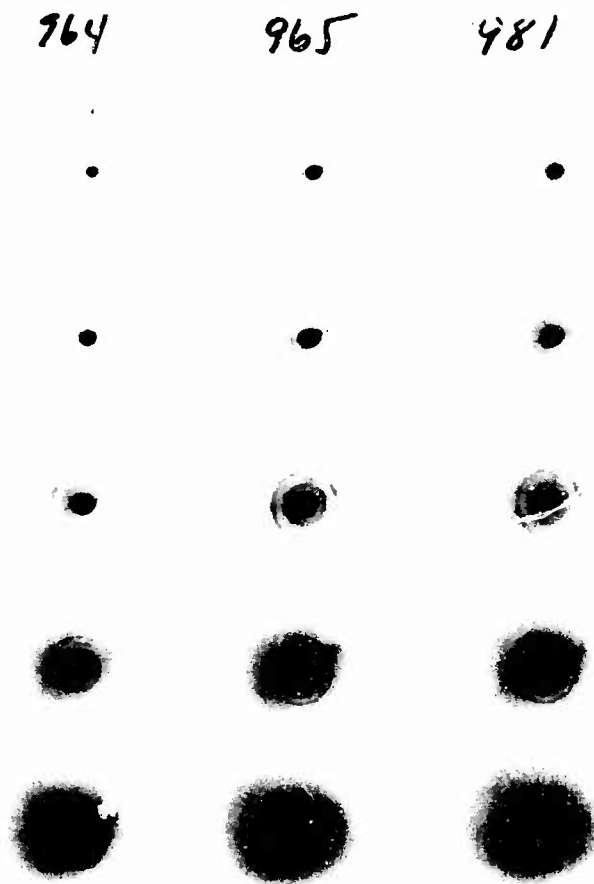Thresholds. Components B are 10% Beam Splitters.

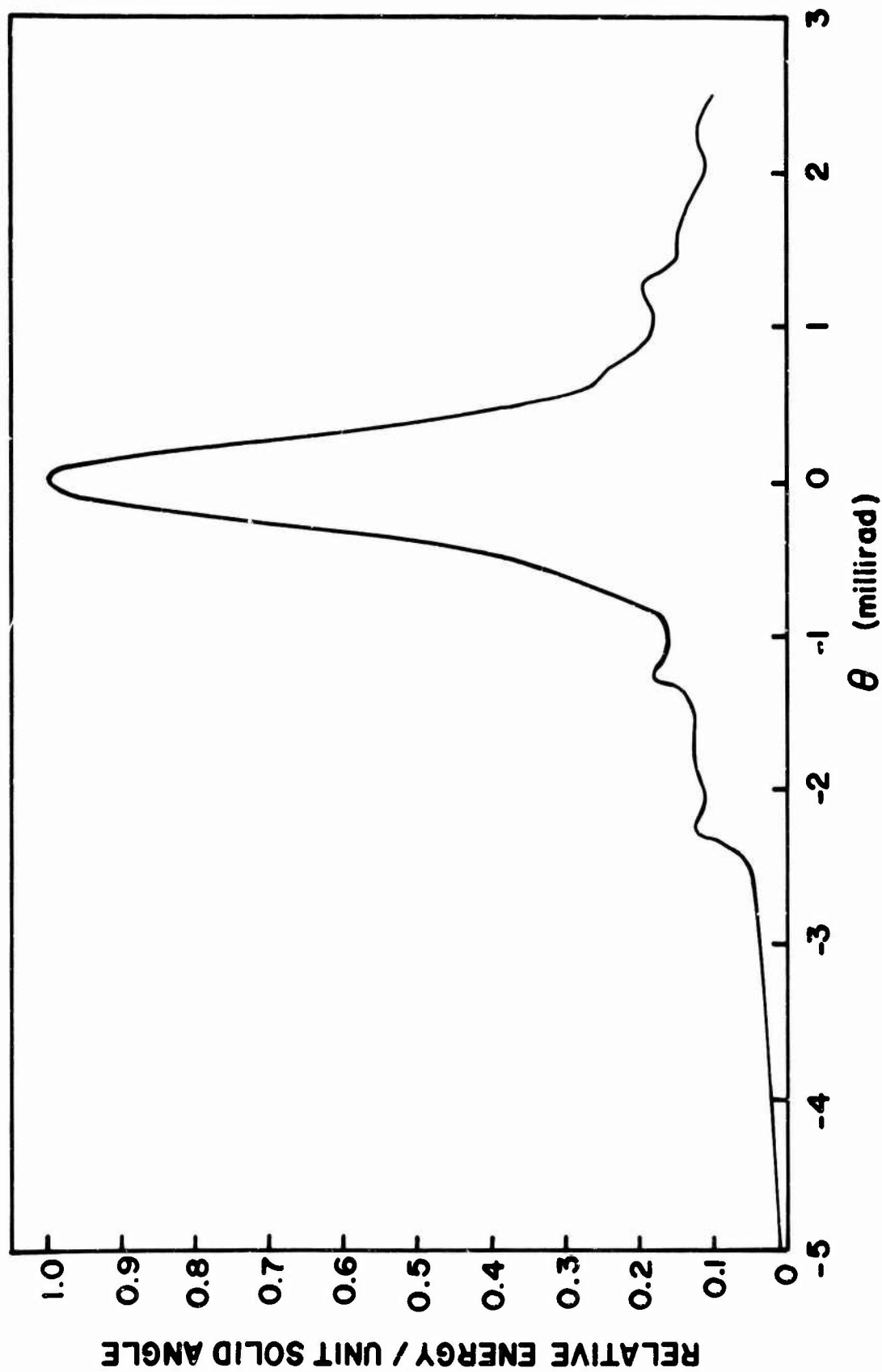Fig. 2.3 Sets of Far-field Patterns for 3 Laser Shots.

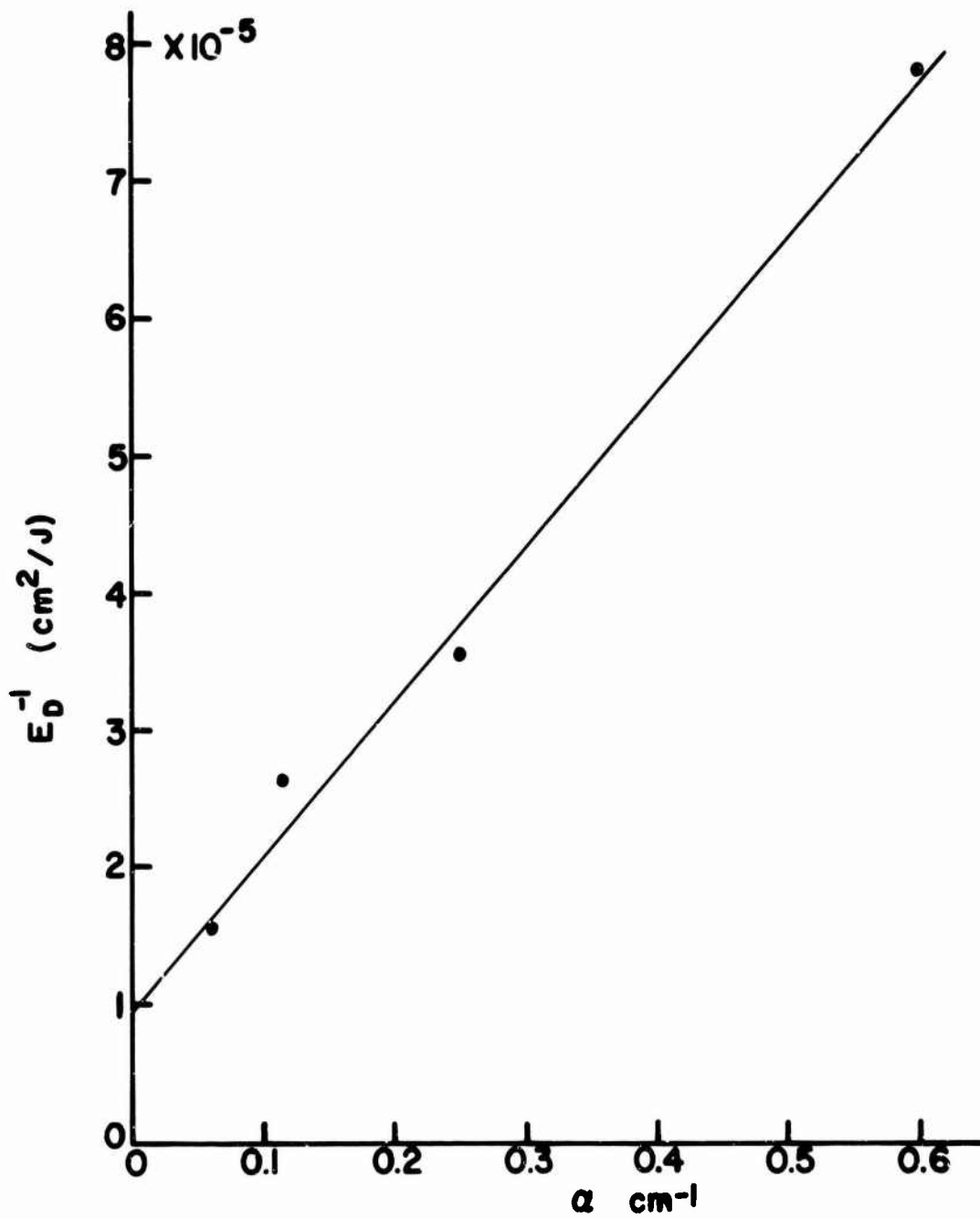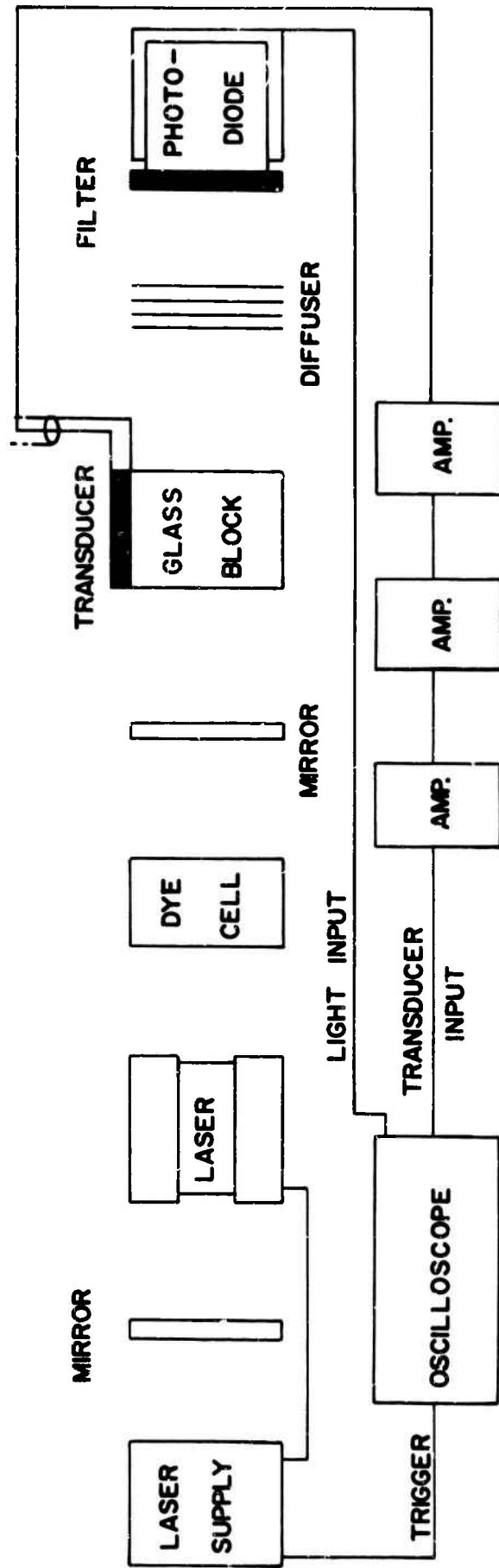Fig. 2.4 Far field Energy Distribution.

Fig. 2.5 Reciprocal of Damage Threshold Versus Absorption
Coefficient for Iron-doped Glasses.
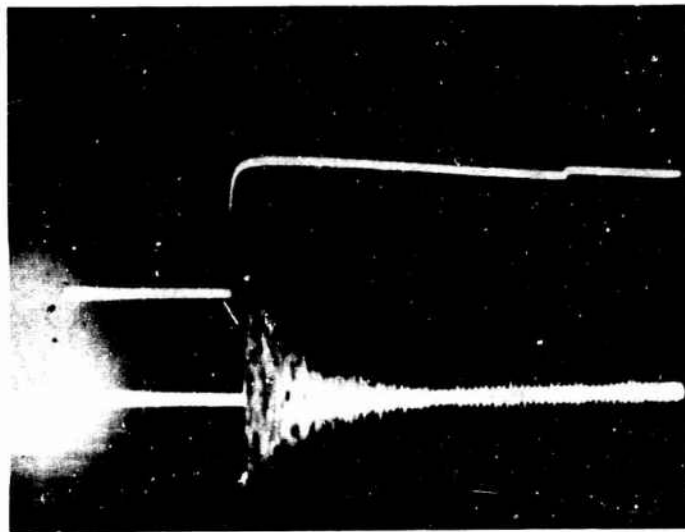
Fig. 2.6 Block Diagram of Apparatus

Fig. 2.7 Integrated Laser Energy (upper trace) Versus Induced Acoustic Signal (lower trace) in a Low Absorption Glass. Sweep, 100 μsec/cm.
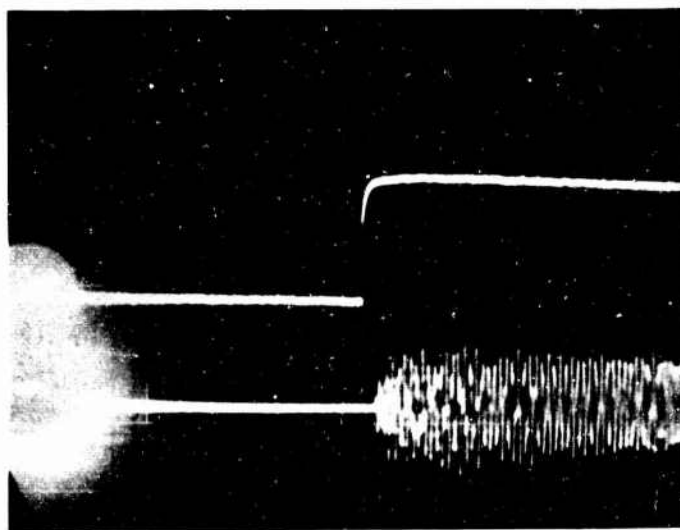
Fig. 2.8 Integrated Laser Energy (upper trace) versus Induced Acoustic Signal (lower trace) in a High Absorption Glass. Sweep, 100 μsec/cm.

Fig. 2.9 Acoustic Pressure Amplitude Per Unit Light Energy
          Density P/E Versus Absorption $A=1-e^{-\alpha l}$ in the 95EV-
          Series Glasses.

Fig. 2.10 Acoustic Pressure Amplitude Per Unit Light Energy
Density P/E Versus Absorption $A=1-e^{-\alpha l}$ in the 95EV-
Series Glasses for large A.

Fig. 2.11 Acoustic Pressure Amplitude Per Unit Light Energy Density P/E Versus $A=1-e^{-\alpha l}$ in the 843KS-KS6 Series Lead Glasses.

Fig. 2.12 Acoustic Pressure Amplitude Per Unit Light Energy Density P/E versus $\alpha A = \alpha(1 - e^{-\alpha l})$ in the 843KS-KS6 Series Lead Glasses.
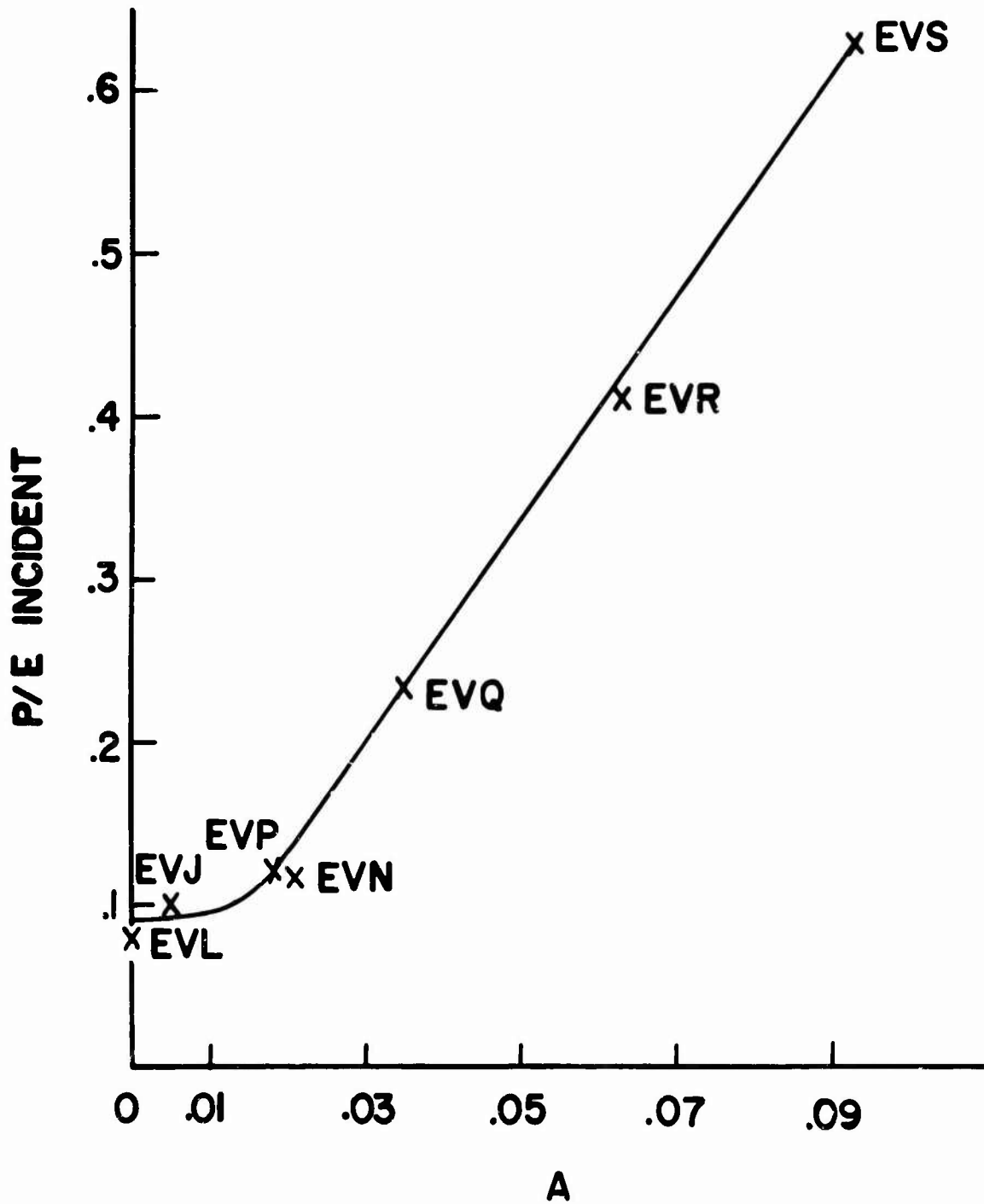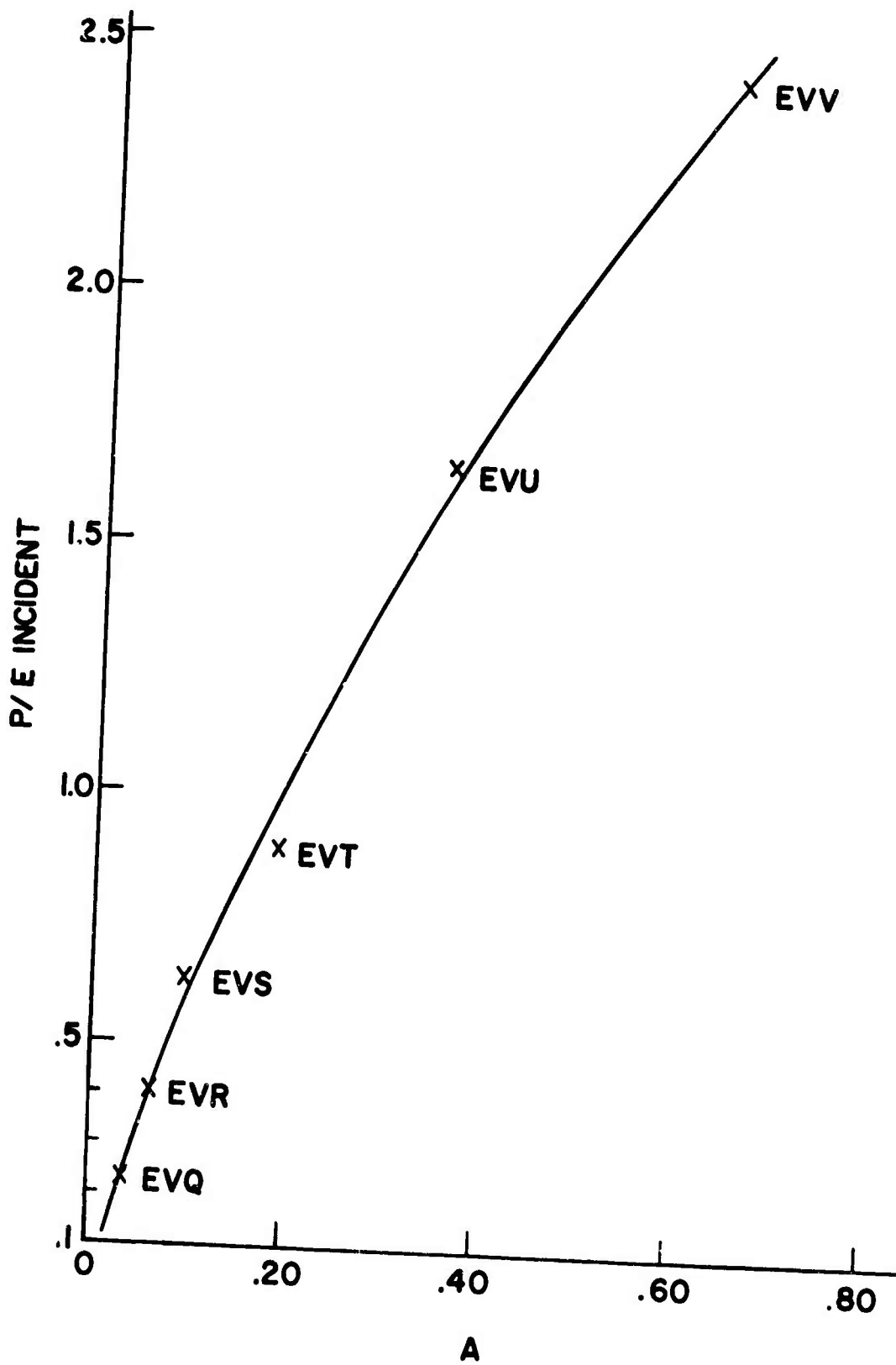
Fig. 2.13 Acoustic Pressure Amplitude Per Unit Light Energy
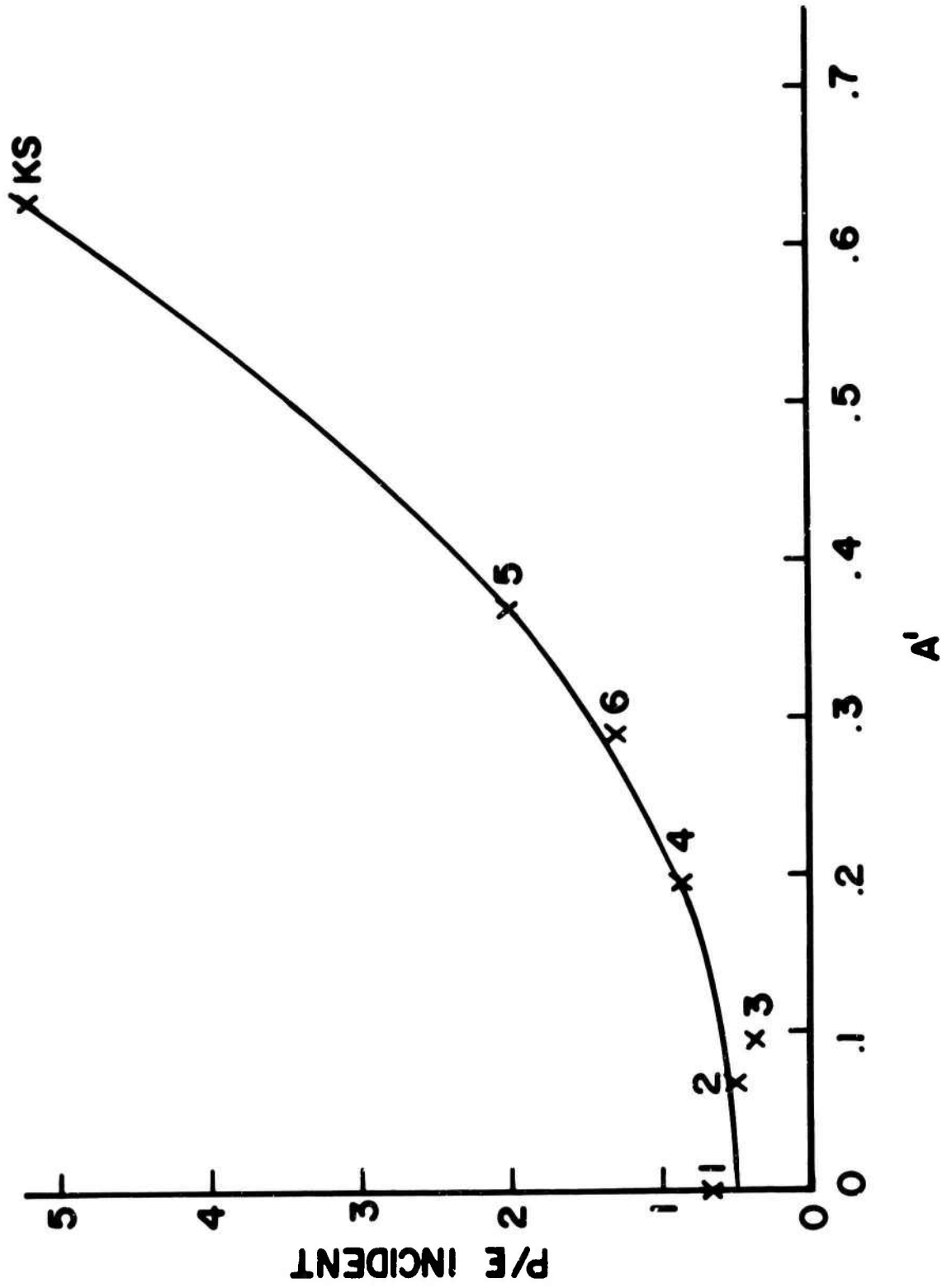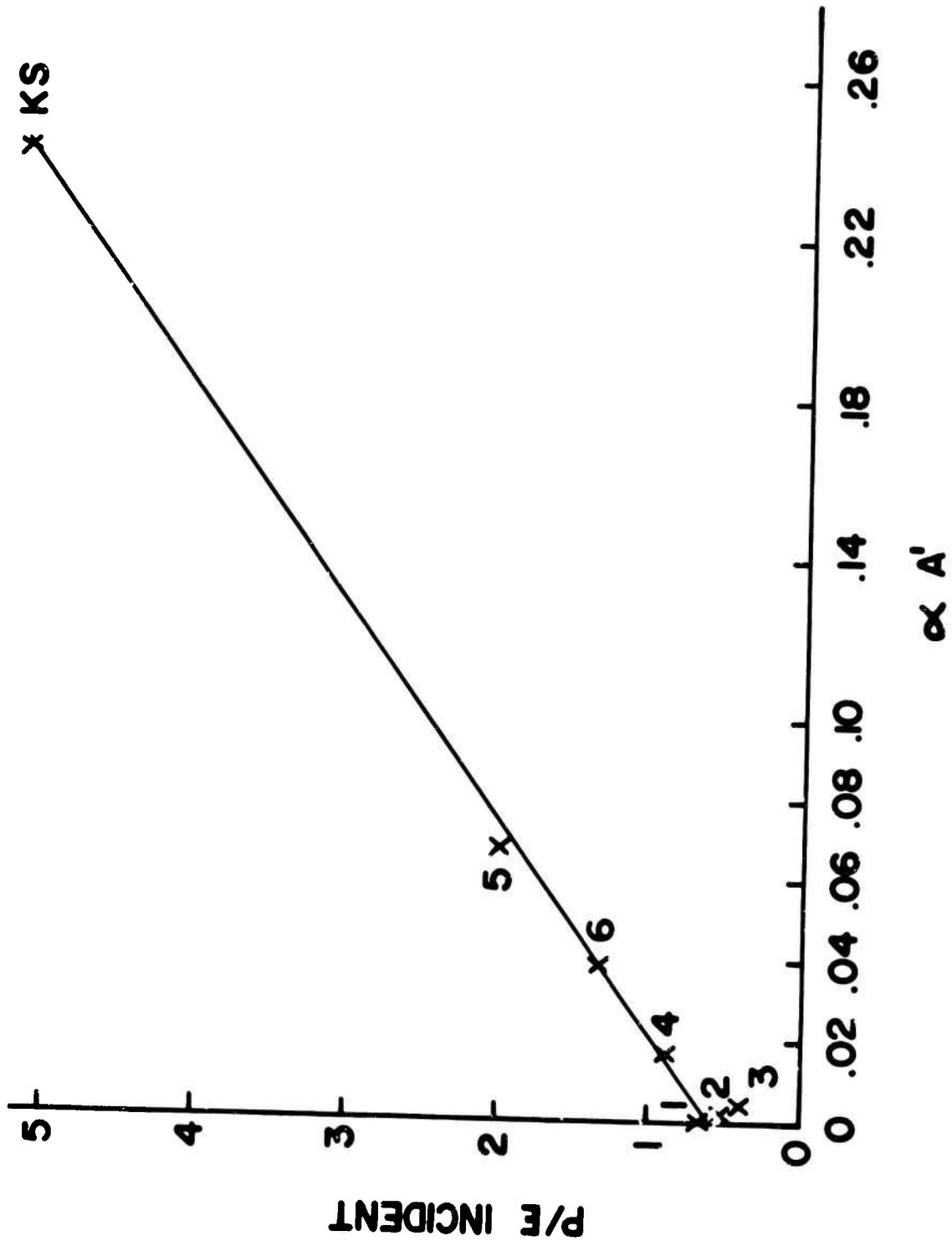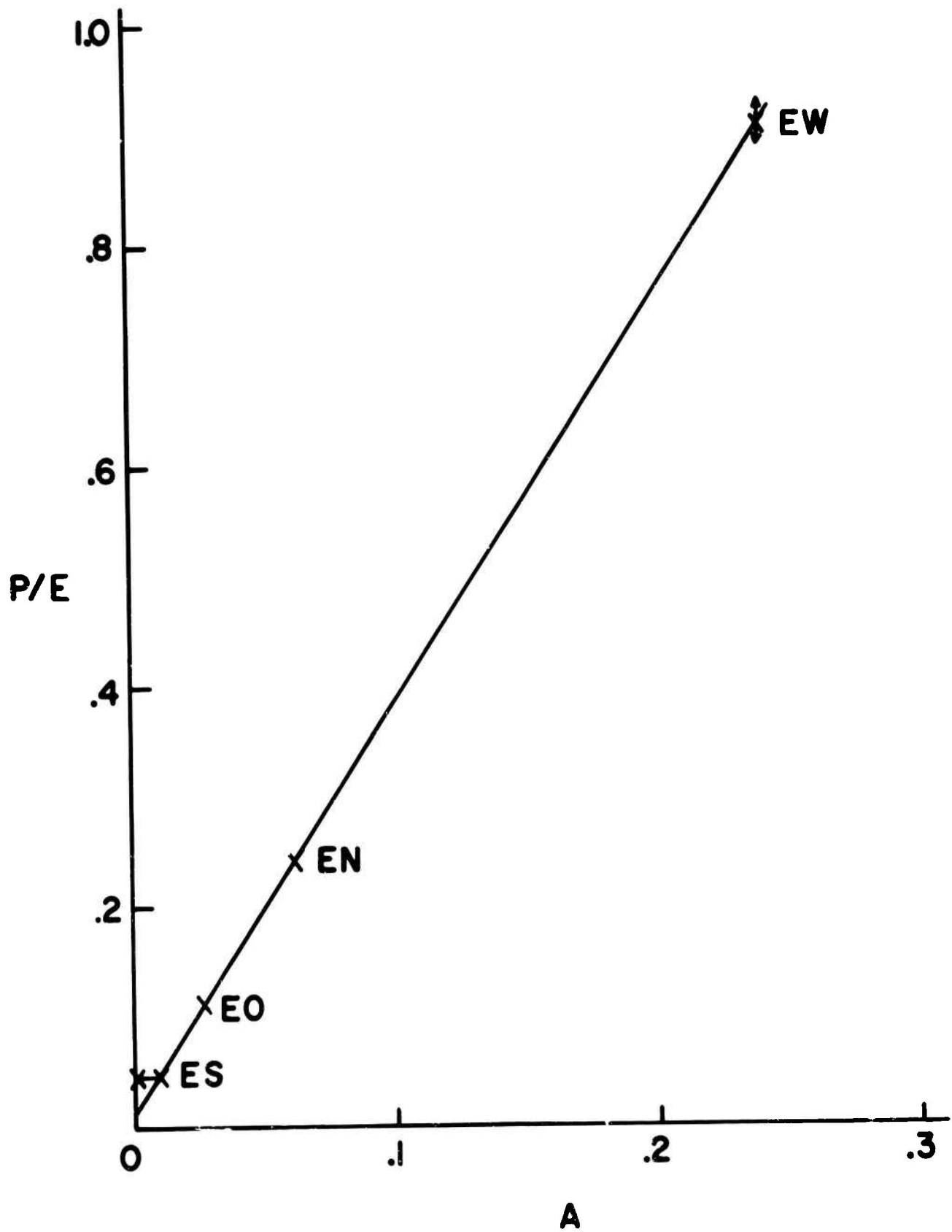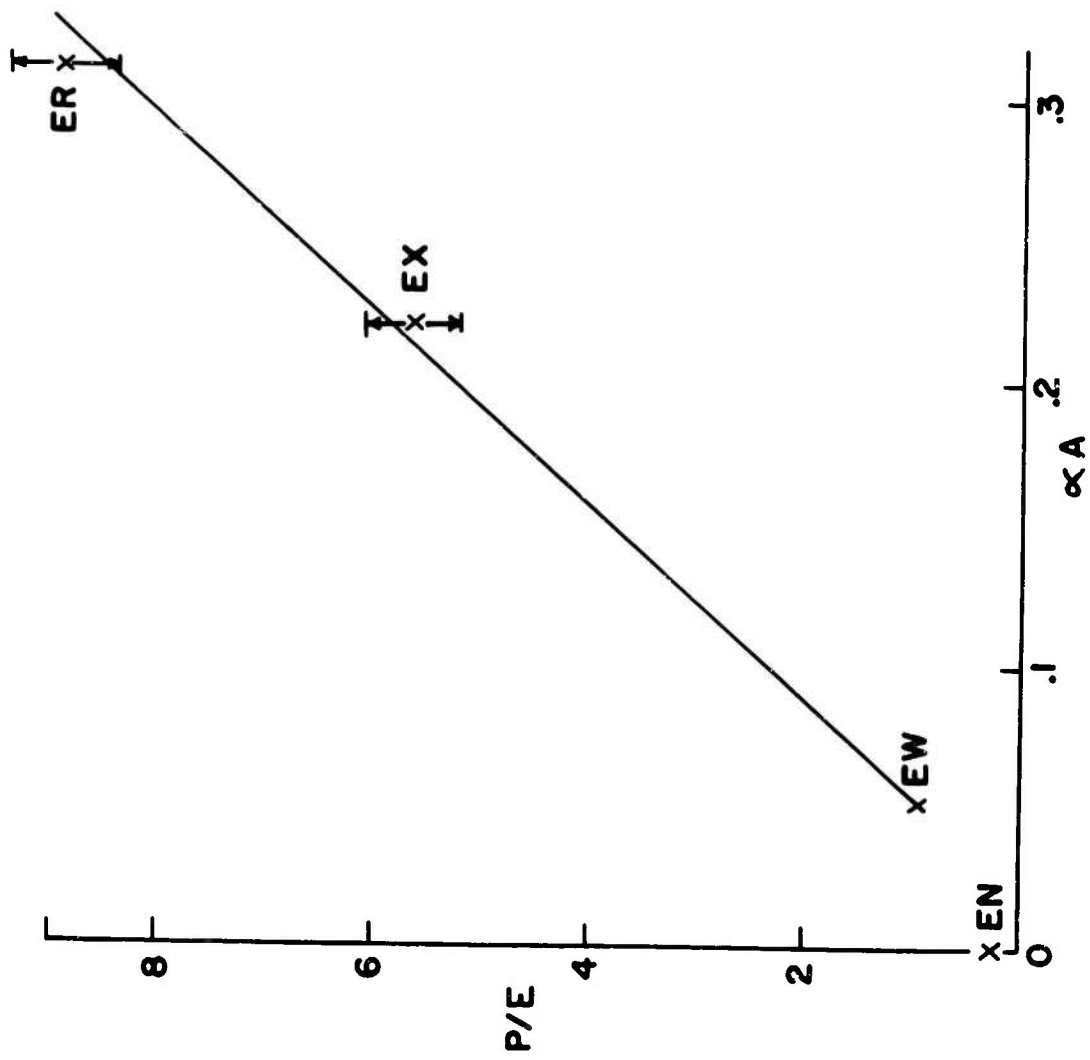Density P/E Versus $A=1-e^{-\alpha l}$ in the 825E-Series Glasses.

Fig. 2.14 Acoustic Pressure Amplitude Per Unit Light Energy Density P/E versus $\alpha A = \alpha(1-e^{-\alpha'})$ in the 825E-Series Glasses.

3. EFFECTS DUE TO OPTICAL ABSORPTION BY NEODYMIUM

3.1 Introduction

Our experiments have shown that the long-pulse damage threshold in neodymium-doped glass decreases as the neodymium concentration is increased and decreases as the sample temperature is increased. These facts support the hypothesis that there is an appreciable absorption of the laser radiation by the neodymium ions themselves. Several possibilities present themselves and will be discussed in terms of the usual four-level system with energy levels 1, 2, 3 and 4 in ascending order of energy. The laser transition is the 3-2 transition. Level 4 is a level in the pump band such that the frequencies ν_{23} and ν_{34} are equal. The possible explanations are:

a) Population of state 3 by conventional optical pumping, followed by 3-4 absorption at 1.06u and dissipative 4-3 radiationless transitions. In the experiments mentioned above, the samples were not optically pumped, but in a previous report we showed both theoretically and experimentally that this is a small effect.[3.1/] Basically, this is limited by the maximum energy per unit volume that can be stored by optical pumping, which is small compared to the energy per unit volume required for damage.

b) Double photon absorption. Sirgh and Geusic have explained the strong nonlinear absorption of 1.06μ light by $NdCl_3$ crystals in terms of two consecutive double photon absorptions.[3.2/] However, we have not observed this type of absorption in neodymium glass.

c) Saturation of the 2-3 transition followed by 3-4 absorption at 1.06µ and 4-3 radiationless transitions. The 2-3 transtion saturates under readily attainable laser intensities. If the temperature is raised by several hundred degrees Centigrade either by means of a furnace or by absorption associated with impurities in the glass, level 2 becomes appreciably populated. By virtue of the condition of saturation, the level 3 population becomes comparable to that of level 2. Then 3-4 absorption of the laser beam is possible if the cross section σ_{34} is appreciable. This absorption depends not on the stored energy density but on the incident energy density and can therefore become comparable with the energy density needed for damage.

d) Thermal quenching of the 3-2 transition. If at elevated temperatures the lifetime of state 3 becomes shorter, it requires greater intensity to saturate the 2-3 transition and more energy is dissipated. The lifetime would have to decrease by two orders of magnitude in order to make this the controlling absorption process. Lifetime measurements here and elsewhere[3.3/] show a slight increase with increasing temperatures up to 450°K. However this effect cannot be ruled out for temperatures much higher than this.

Since process (c) seemed to be the most likely source of absorption it was decided to determine the size of the effect and, if possible, measure σ_{34}.

3.2 Theory of Saturation and Excited State Absorption in Neodymium Glass

The energy level diagram for Nd^{3+} in soda-lime glass appears in Figure 3.1.[3.4/] The $^4G_{9/2}$ level assigned by Dieke and Pardey[3.5/] is sufficiently broad in the glass to make 1.06μ 3-4 transitions plausible. The g-values were determined by Borrelli who found it necessary to assume g=4 for each of the $^4F_{3/2}$ levels to get agreement between fluorescence data and absorption data.[3.6/]

3.2.1 The Population of Level 2

Since the effect we are describing becomes important only at elevated temperatures, we compute the population density n_2^o of the lower level 2 as a function of temperature, assuming thermal equilibrium, from the relation

$$n_2^o = \frac{n_o g_2 \exp(-h\nu_{21}\, 1/kT)}{\sum_i g_i \exp(-h\nu_i 1/kT)}$$

$$= n_o \left[\frac{4}{6} \exp\left(\frac{2810}{T}\right) + \frac{6}{6} \exp\left(\frac{2263}{T}\right) + 1 + \frac{6}{6} \exp\left(\frac{-380}{T}\right) \right]^{-1} \quad (1)$$

where all four of the $^4I_{9/2}$ and $^4I_{11/2}$ levels have been included while higher levels may be neglected for the temperatures of interest here. The population density n_o is total ion population and T is the absolute temperature. Table I gives computed values n_2^o/n_o for various temperatures.

Table I

Computed Value of n_2/n_o for Several Temperatures

T ($^\circ$K)	n_2^o/n_o
300	0.000103
500	0.00359
700	0.0158

3.2.2 Saturation in a Two-Level System with Fixed Lower-State Population

The four transitions between $^4F_{3/2}$ and $^4I_{11/2}$ are of the order of $200cm^{-1}$ full width at half height. Hence 1.06μ radiation is absorbed via all four transitions, but most strongly via 2-3 and 2'-3'. Levels 2 and 2' are thermally connected and levels 3 and 3' are thermally connected. The exact solution to the saturation problem thus involves all four levels and requires some quantitative data on lattice relaxation ratio. However, since the resonant transition 2-3 is the strongest of the group, we expect to be in error by less than a factor of 2 if we simply make the calculation for the 2-3 transition. Since spectral cross-relaxation is fast, we can treat the levels as if they were homogeneously broadened.[3.7,3.8]

The level scheme simplifies to that shown in Figure 3.2. The rate equations at steady state give:

$$\dot{n}_3 = n_2(W_{23}^i + W_{23}^l) + n_3(-W_{32}^i - W_3) = 0$$

$$n_2 = n_2^o \tag{2}$$

where W_{23}^i and W_{32}^i are induced transition rates, W_{23}^l is the upward lattice relaxation rate and W_3 is the transition rate from the upper state to all other states by radiative and nonradiative means. We set n_2 equal to the thermal equilibrium value n_2^o because state 2 is in thermal equilibrium with the ground state and the ground-state population is depleted by only a few per cent when the 2-3 transition becomes saturated. In thermal equilibrium the rate equations are:

$$\dot{n}_3 = n_2(W_{23}^l) + n_3(-W_3) = 0$$

$$n_2 = n_2^o. \tag{3}$$

Using the relation $g_3 W_{32}^i = g_2 W_{23}^i$, we obtain from these rate equations the following expression for the ratio of 2-3 absorption coefficient in the presence of radiation to the 2-3 absorption coefficient under conditions of thermal equilibirum:

$$\frac{\alpha_{23}(\nu)}{\alpha_{23}^o(\nu)} = \frac{n_2^o - \frac{g_2}{g_3} n_3}{n_2^o - \frac{g_2}{g_3} n_3^o} = \frac{1}{1 + \frac{W_{32}^i}{W_3}} . \tag{4}$$

The saturation parameter K is the intensity at which this ratio becomes $\frac{1}{2}$, i.e. $W^1_{32} = W_3$. Since

$$W^1_{32} = B_{32} \ w(\nu) \ d\nu \ S(\nu), \tag{5}$$

$$B_{32} = \frac{g_2}{g_3} \ \frac{v}{h\nu \ n^o_2} \int \alpha^o_{23}(\nu) \ d\nu, \ n^o_3 \cong 0, \tag{6}$$

and

$$S(\nu) = \frac{\alpha^o_{23}(\nu)}{\int \alpha^o_{23}(\nu) d\nu} , \tag{7}$$

where B_{32} is the Einstein coefficient, $w(\nu)d\nu$ is the energy density within frequency element $d\nu$, v is the light velocity in the medium, and $S(\nu)$ is the normalized shape function of the absorption line for $n^o_3 \approx 0$, we have finally

$$v \ w(\nu)d\nu = K$$
$$= g_3 \ n^o_2 \ h\nu \ W_3/g_2 \ \alpha^o_{23}(\nu). \tag{8}$$

Equation (4) now becomes

$$\frac{\alpha_{23}(\nu)}{\alpha^o_{23}(\nu)} = \frac{1}{1 + \frac{I}{K}} \tag{9}$$

where I is the radiation intensity at frequency ν.

3.2.3 Calculation of the Total Absorption at 1.06 Microns

Equations (4) and (9) describe the population of level 3 as a function of intensity. The absorption coefficient for the postulated 3-4 absorption is by definition

$$\alpha_{34} = \sigma_{34} \ (n_3 - \frac{g_3}{g_4} \ n_4), \tag{10}$$

where σ_{34} is the absorption cross section. We can assume that the nonradiative 4-3 transitions are fast so that $n_4 \ll n_3$. Also $n_3^o \ll n_2^o$. Equations (4), (9) and (10) then yield

$$\alpha_{34} = (g_3/g_2) \, n_2^o \, \sigma_{34} \, (1 + K/I)^{-1}. \tag{11}$$

From Equation (4) we also obtain α_{23}, so that the total absorption coefficient at 1.06 microns as a function of the intensity is

$$\alpha(I) = \alpha_{23} + \alpha_{34} = \frac{n_2^o \, \sigma_{23}}{1 + I/K} \left[1 + \frac{g_3 \, \sigma_{34} \, I}{g_2 \, \sigma_{23} K} \right]. \tag{12}$$

The limiting conditions $I = 0$ and $I = \infty$, which are approximately realizable experimentally, yield values of σ_{23} and σ_{34}, respectively:

$$\lim_{I \to 0} \left[\alpha(I) \right] = n_2^o \, \sigma_{23} \tag{13}$$

$$\lim_{I \to \infty} \left[\alpha(I) \right] = (g_3/g_2) \, n_2^o \, \sigma_{34} . \tag{14}$$

The transmittance I/I_o of a sample of length χ is obtained by integrating the equation

$$\frac{dI}{I \, \alpha(I)} = - \, dx \quad , \tag{15}$$

the solution of which is

$$\frac{I}{I_o} \left[\frac{aK + I}{aK + I_o} \right]^{a-1} = \exp (-\alpha_{23}^o \, x), \tag{16}$$

$$\text{where} \quad a = \frac{g_2 \, \sigma_{23}}{g_3 \, \sigma_{34}} \tag{17}$$

and K is the saturation parameter given by Equation (8).

3.3 Measurement of σ_{34}

It is not feasible to measure σ_{34} by measuring the excited-state absorption under optical pumping because the absorption is overcome by the gain of the medium. However, this difficulty is avoided if state 3 is populated by 2-3 saturation at an elevated temperature, as shown by Equations (13) and (14). Figure 3.3 indicates the experimental arrangement for doing this. The laser was operated at constant output energy as described in Section 2.3 in order to keep the bandwidth, pulse shape, and relative energy distribution constant. The beam was then suitably attenuated with calibrated filters. In order to greatly exceed the saturation parameter K, it was necessary to place the 10cm sample (Code 0580 Laser Glass) in the focal region of a 50cm focal length lens. With this long focal length the non-uniformity in beam cross-section along the sample was not serious. The beam intensity was measured in front of and behind the sample by means of photomultipliers as shown in the figure. The time traces were displayed and photographed on an oscilloscope for each shot. The essentially steady-state intensity ratios at the peaks of the pulses were measured at room temperature for a wide range of intensities. Then the sample temperature was raised to about 700°K and the measurements were repeated. After the sample had returned to room temperature, the ratios were rechecked and found to be reproducible. Since no intensity dependence of sample transmittance

was found at room temperature, and since the absorption of the
sample was very small at room temperature, it was convenient
to take the 700°K intensity ratio divided by the room temperature
ratio as the transmittance I/I_o for the elevated temperature.

The resulting transmittances are shown in Figure 3.4
plotted versus I_o/K. The unsaturated value is 0.575 and partial
saturation is evident at higher intensities. The theoretical
curves were calculated from Equations (12)-(17) as follows.
Because, as seen in Fig. 2.4, a large proportion of the energy
falls outside the beam half-width, it was necessary to compute
the theoretical transmittance separately for each element of
cross-sectional area. An effective transmittance I/I_o was then
obtained by weighting and summing. The value of K for this glass
is 4.13×10^4 W/cm^2, calculated from Equation (8) with $g_3/g_2 = 4/6$,
$h\nu = 2 \times 10^{-19}$ J, $1/W_3 = 320 \times 10^{-6}$ sec, $\alpha_{23}^o/n_2^o = \sigma_{23} = 1 \times 10^{-20}$ cm^2.
Theoretical curves for $\sigma_{34}/\sigma_{23} = 0$, 0.5, and 0.75 are drawn in
the figure. The experimental points appear to agree quite well
with the curve for $\sigma_{34}/\sigma_{23} = 0.75$. This is probably an upper
limit to the 3-4 cross section for two reasons. First, any other
temperature-dependent absorptive effect would tend to lower the
transmittance also and lead to too high values of σ_{34}. Temperature
quenching, mentioned earlier, should be investigated in this
connection. Second, any geometrical effects which make the
intensity within the sample less than what it is thought to be
(e.g. variation in beam half-width along the length of the sample)

decrease the effective I/I_o and exaggerate the value of σ_{34}. Third, if we have underestimated the value of K somewhat, the value of σ_{34} obtained is slightly high. However, it seems probable that σ_{34} is of the order of 0.5 σ_{23}. A more precise value can be obtained by eliminating the periphery of the laser beam so that nearly complete saturation can be attained.

④ $^4G_{9/2}$ 21100 cm^{-1}

③ $^4F_{3/2}$ 11530   3' _____   2 (THEO.),4(EXP.)
              11370   3 _____   2   ,4

1.06μ

② $^4I_{11/2}$ 2210   2' _____   6
           1950   2 _____   6

① $^4I_{9/2}$ 380   1' _____   6
          0   1 _____   g=4

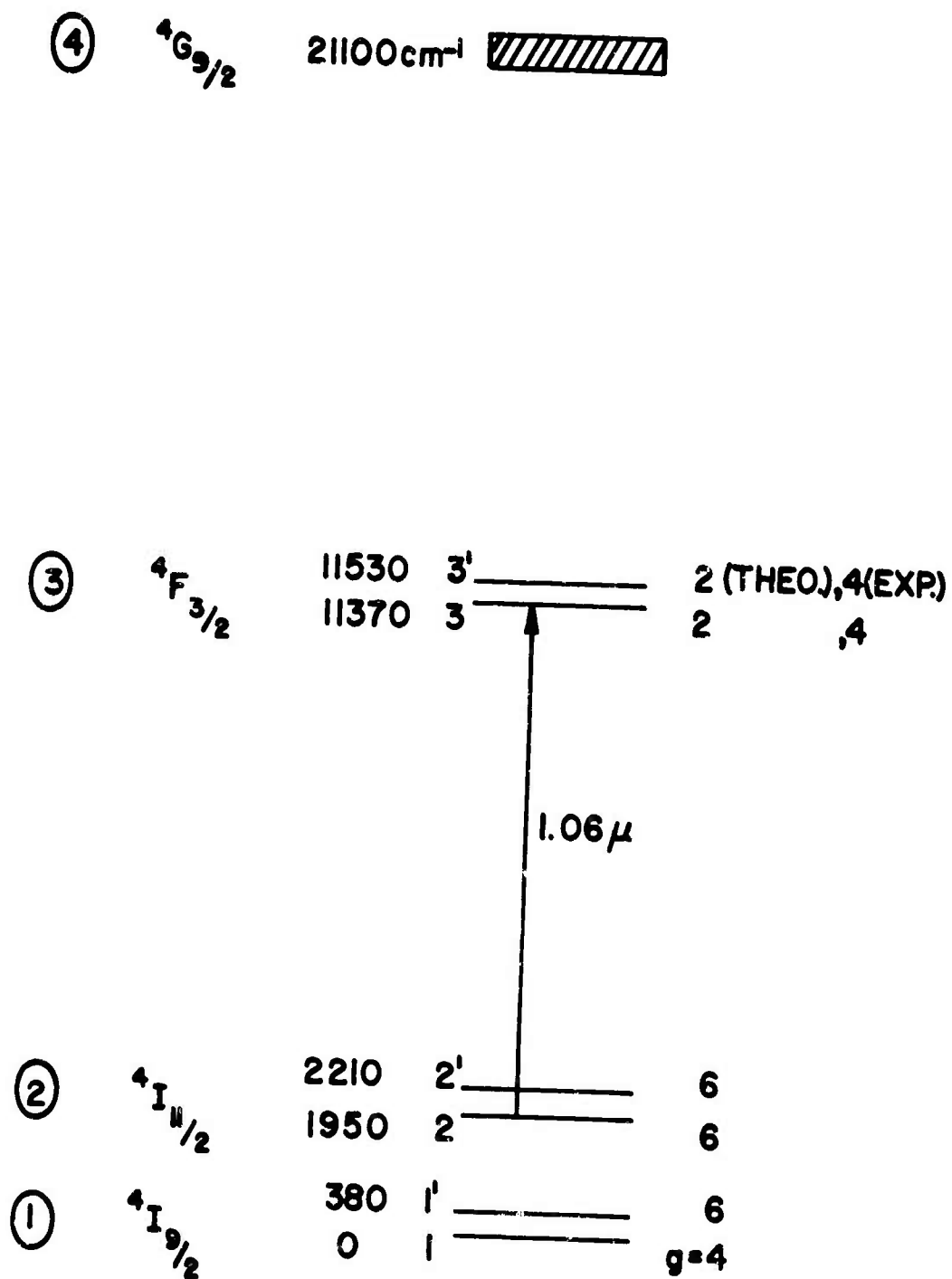Fig. 3.1   Energy Level Diagram of Nd^{3+} in Soda-lime Glass[4]. Level 4 Energy from Reference 5. Degeneracies from Reference 6.
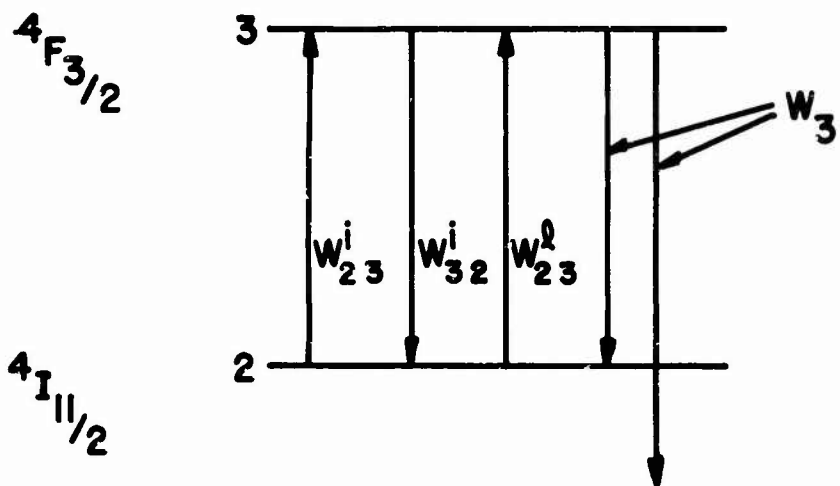
Fig. 3.2   Two-level System Illustrating Transition Rates.
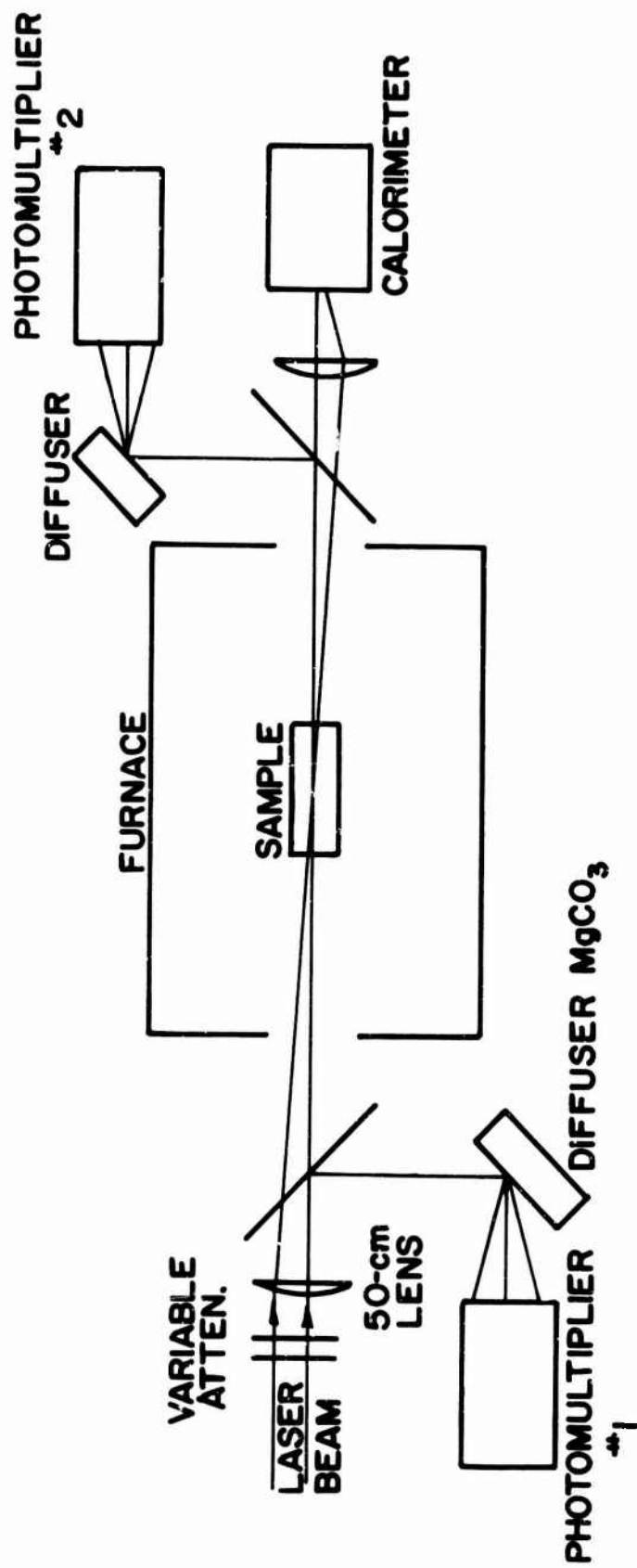
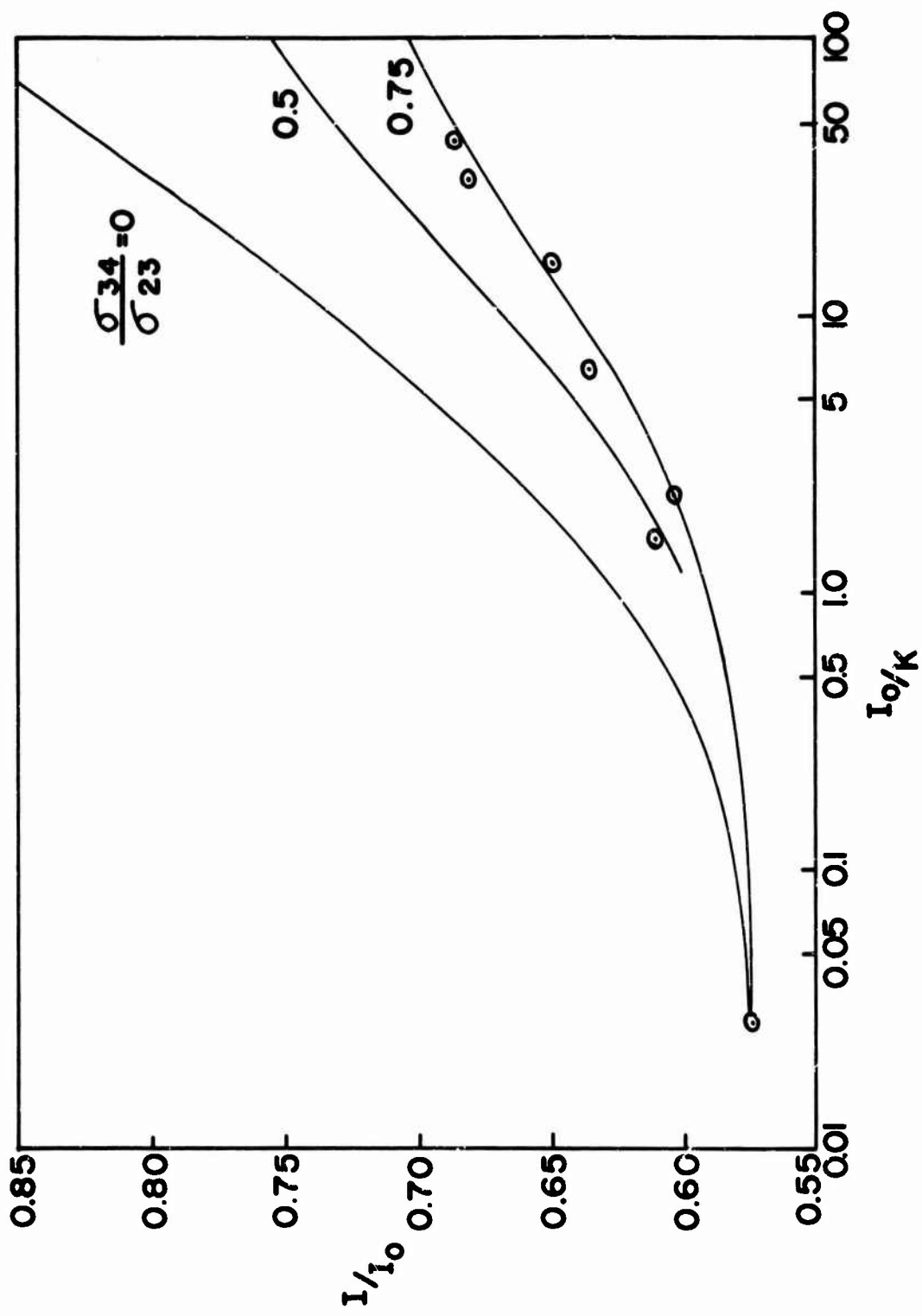Fig. 3.3 Experimental Arrangement for Measuring σ_{34} in Neodymium Glass.

Fig. 3.4 Theoretical and Experimental Saturation Curves.
Solid Curves are Calculated for $\sigma_{34}/\sigma_{23} = 0, 0.5$, and
0.75.

4. MEASUREMENT OF THE OPTO-ACOUSTIC COUPLING RELATED TO THE
CAUSE OF GLASS DAMAGE

4.1 Introduction

As was demonstrated before in Section 2.3, elastic
waves are produced in non-absorbing media due to the passage of
a laser beam. This effect, giving rise to a different type of
opto-acoustic coupling than that treated in Section 2.3 for
absorbing media, will be discussed as an intrinsic effect
characteristic of a laser beam in a material medium, and may
arise as a result of electrostrictive mixing of laser beam
frequency components. Electrostriction may act as a nonlinear
mechanism to mix the various frequency components of a single
laser beam which are present in its bandwidth and give rise to
an elastic wave traveling in the medium. Kastler[4.1/] has
calculated the amplitude of a pressure wave generated in a fluid
by the electrostrictive coupling between two light beams.
Kastler's solution, which was one-dimensional, was for the steady-
state case, and predicted large pressure amplitudes for certain
angles of intersection of the light beams. This characteristic
of the solution arises because of its steady-state nature - the
intersection of the light beams produces a moving system of
interference fringes which, if the angle of intersection is
properly chosen, will propagate at the velocity of sound in the
medium. Then the wave will build up in time, reaching a value
limited by the losses in the medium. In the transient case,

which will be considered here, no such "resonance" exists because the laser beam will be assumed to exist for a time $t \ll 2\pi/\Omega$, where Ω is the angular frequency of the generated elastic wave. It is desired to find the dependence of the induced pressure amplitude on laser beam intensity, bandwidth, and duration as well as on the properties of the medium. A calculation, based on elementary methods, follows. Rationalized mks units are used except where otherwise indicated.

4.2 Electrostrictive Generation of Elastic Waves

4.2.1 Calculation of the Effect

Kastler[4.1] has derived the equation of motion of a fluid due to electrostrictive beam mixing; it will be briefly repeated here for the sake of clarity. The electric field of two plane light waves superposed is given by

$$E = E_1 \cos(\omega_1 t - k_1 \cdot r) + E_2 \cos(\omega_2 t - k_2 \cdot r), \tag{19}$$

where ω and k are their angular frequencies and wave vectors, respectively, and t is the time.

Assuming the polarizations parallel, and $|E_1| = |E_2| = E_o$, one has

$$E = 2E_o \cos\left[\left(\frac{\omega_1 - \omega_2}{2}\right)t - \left(\frac{k_1 - k_2}{2}\right)\cdot r\right] \cos\left[\left(\frac{\omega_1 + \omega_2}{2}\right)t - \left(\frac{k_1 + k_2}{2}\right)\cdot r\right] \tag{20}$$

We are interested in the term involving $\omega_1 - \omega_2$, as the medium cannot follow variations as rapid as $\omega_1 + \omega_2$.

The electrostrictive pressure generated by the passage of the superposed light beams is given by

$$P = \gamma \; E^2 = \tfrac{1}{2} \rho \; \frac{d\epsilon}{d\rho} E^2, \tag{21}$$

where ρ is the density and ϵ the dielectric constant.

The constant γ is derived from the Clausius-Mosotti relation as

$$\gamma = \frac{\epsilon_o}{6} (n^2-1)(n^2+2), \tag{22}$$

where ϵ_o is the dielectric constant of free space and n is the index of refraction, taken as the square root of the relative dielectric constant.

Squaring Eq. (20), and introducing the time average of the term $\cos^2 \left(\frac{\omega_1 + \omega_2}{2} \right) t \ldots$ brings in a factor of $\tfrac{1}{2}$, leaving

$$E^2 = E_o^2 + E_o^2 \cos \left[(\omega_1-\omega_2)t - (k_1-k_2) \cdot r \right], \tag{23}$$

so that the time-varying part of the electrostrictive pressure driving the fluid is given by Eq. (21) as

$$P = \gamma E_o^2 \cos \left[(\omega_1-\omega_2)t - (k_1-k_2) \cdot r \right],$$
$$= \gamma E_o^2 \cos \Omega (t - \frac{x}{c}); \tag{24}$$

and the difference frequency Ω appears.

The solution to the problem at hand is found from the Navier-Stokes equation in one dimension,

$$\rho_o \; \frac{\partial^2 \zeta}{\partial t^2} = - \; \frac{\partial P}{\partial X} + \left[\frac{4}{3} \eta - \eta' \right] \frac{\partial^3 \zeta}{\partial X^2 \partial t} + \frac{+\partial F}{\partial X} . \tag{25}$$

Here ζ is the particle displacement, η and η' are viscosity coefficients, and F is any forcing function such as Eq. (24).

Since we seek a transient solution for which $(\omega_1 - \omega_2) t \ll 1$, losses due to viscosity may be neglected as an approximation, and we set $\eta = \eta' = 0$. The solution thus obtained will therefore differ from that of Kastler, who did not neglect the viscosity.

Making use of the acoustic impedance ρC, where C is the velocity of elastic wave propagation,

$$P = \rho C \ \frac{\partial \zeta}{\partial t} .$$

$$(26)$$

Since ζ is of the general form

$$\zeta = \zeta_o \ e^{\pm \ i(\nu t - x/\lambda)},$$

$$(27)$$

we see that

$$\frac{\partial \zeta}{\partial t} = \pm i \nu \zeta, \quad \frac{\partial \zeta}{\partial X} = \mp \frac{1}{\lambda} \zeta.$$

$$(28)$$

Thus

$$\frac{\frac{\partial \zeta}{\partial t}}{\frac{\partial \zeta}{\partial X}} = - C,$$

$$(29)$$

so that

$$P = \rho C \ \frac{\partial \zeta}{\partial t} = - \rho C^2 \ \frac{\partial \zeta}{\partial X} .$$

$$(30)$$

Then Eq. (25) becomes

$$\frac{\partial^2 \xi}{\partial t^2} = C^2 \frac{\partial^2 \xi}{\partial X^2} - \frac{\Omega}{\rho C} \gamma E_o^2 \sin \Omega(t - \frac{x}{C}), \tag{31}$$

or

$$\frac{\partial P}{\partial t} = - C \frac{\partial P}{\partial X} + \Omega \gamma E_o^2 \sin \Omega(t - \frac{x}{C}). \tag{32}$$

In order to evaluate the relative magnitude of the first two terms, suppose P rises from zero to 10^3 dynes/cm^2 in 10^{-8} sec, as can happen experimentally with a Q-switched laser. Then if $\Omega = 6 \times 10^6$ rad/sec, $C \sim 5 \times 10^5$ cm/sec,

$$\frac{\partial P}{\partial t} \sim 10^{11},$$

and

$$C \frac{\partial P}{\partial X} \sim 10^9.$$

We thus can neglect the term in $\partial P/\partial X$ as a first approximation for low frequencies, obtaining

$$\frac{\partial P}{\partial t} = \gamma \Omega E_o^2 \sin \Omega(t - \frac{X}{C}). \tag{33}$$

Expanding the cosine as a sum of two angles and keeping in mind that $\Omega t \ll 1$, we have

$$\frac{\partial P}{\partial t} = \gamma \Omega E_o^2 \sin \frac{\Omega X}{C} + \gamma \Omega^2 t E_o^2 \cos \frac{\Omega X}{C}. \tag{34}$$

We see that we must have the solution

$$P = \gamma \Omega \sin \frac{\Omega X}{C} \int_o^t E_o^2 \, dt + \gamma \Omega^2 \cos \frac{\Omega X}{C} \int_o^t E_o^2 \, t dt \tag{35}$$

For a general point in space, where $\frac{\Omega X}{C}$ does not take on a special value such as $\frac{\Omega X}{C} = \pi$, the first term predominates, and the solution grows linearly in time if the laser is switched on (so I = constant) at t = 0. We note immediately that the solution predicts a pressure rich in high-frequency components in contrast with the character of the solution for the generation of elastic impulses by means of absorption. In addition, the effect should increase rapidly with index of refraction, increase linearly with the laser beam intensity, and the elastic waves are generated uniformly in the volume of the medium. For laser intensities which are not constant, the integral of Eq. (35) can be evaluated, as $\int I dt$, where I is the laser beam intensity, is easily found experimentally.

4.2.2 Effect of Laser Bandwidth

The result, Eq. (35), predicts the acoustic pressure amplitude generated on mixing two equal E vector components E_o differing in frequency by $\Omega/2\pi$. Since a real laser beam contains many frequency components i,j... differing in frequency by amounts f_{ij} corresponding to acoustic frequencies, many simultaneous acoustic waves will be generated by the passage of a single Q-switched laser beam.

Let us assume that the laser distribution of intensity versus frequency is Gaussian, with unit integrated intensity and bandwidth ϵ. (Thus half the intensity will be present in frequencies $f < \epsilon$ around f_o, the center or laser

frequency.) Then we may write

$$I(f) = \frac{.48}{\pi^{\frac{1}{2}}\epsilon} \; e^{- \frac{(.48)^2 \, (f-f_o)^2}{\epsilon^2}} . \tag{36}$$

The corresponding density of electric vectors
is given by

$$E = \frac{377(2) \; (.48)}{n\pi^{\frac{1}{2}} \, \epsilon} \; e^{\frac{-(.48)^2 \, (f-f_o)^2}{2\epsilon^2}} . \tag{37}$$

We need now to consider pairs of E vectors E_i,
E_j near to each other in frequency but differing by f_{ij}.
In general,

$$E_i = E_j + \frac{dE}{df} \, f_{ij} . \tag{38}$$

The mixed product $E_i E_j$ summed over i,j is desired;
it takes the form

$$\sum_{i,j} E_i E_j = \sum_{j} E_1 E_j + \sum_{i,j} E_j \, \frac{dE}{df} \, f_{ij} . \tag{39}$$

For a continuous distribution, we must replace
the sums by integrals, and obtain the self-mixing of the beam:

$$\int_{-\infty}^{\infty} E_i E_j \, d(f-f_o) = \int_{-\infty}^{\infty} E^2 \, d(f-f_o) + f_{ij} \int_{-\infty}^{\infty} E \, \frac{dE}{df} \, d(f-f_o) . \tag{40}$$

Inserting the value of E from Eq. (37) and
evaluating the integrals we obtain

$$f_{ij} \int_{-\infty}^{\infty} E \, \frac{dE}{df} \, d(f-f_o) = - \frac{(.48) \, 377}{n\pi^{3/2}} \; \frac{\Omega}{\epsilon} , \tag{41}$$

and

$$\int_{-\infty}^{\infty} E^2 \, d(f-f_o) = \frac{754}{n} \tag{42}$$

Thus the value of the mixing integral per unit laser intensity is

$$\int_{-\infty}^{\infty} E_i E_j \, d(f-f_o) = \frac{754}{n}\left(1 - .043 \frac{\Omega}{\epsilon}\right).$$ (43)

Since $\Omega \ll \epsilon$ is implied in Eq. (38), we may take the result as $754/n$. Inserting this in Eq. (35) we have finally the result for the pressure induced

$$P = \frac{754 \, \gamma\Omega}{n} \sin \frac{\Omega X}{C} \int_o^t I dt + \frac{754 \, \gamma\Omega^2}{n} \cos \frac{\Omega X}{C} \int_o^t I t \, dt,$$

$$\approx \frac{754 \, \gamma\Omega}{n} \sin \frac{\Omega X}{C} \int_o^t I dt.$$ (44)

We see that the passage of a Q-switched laser beam through a medium will give rise to an elastic wave(s) regardless of the presence of optical absorption. In the absence of absorption, the elastic pulse generated is rich in high-frequency components in comparison with the case of high absorption; in both cases, the induced pressure amplitude is proportional to $\int_o^t I dt$, but strongly dependent on the index of refraction in the case of electrostriction. In general, for samples that exhibit small absorption, the elastic waves are generated uniformly in the volume of the medium which is illuminated by the laser beam.

4.2.3 Stimulated Brillouin Scattering

Stimulated Brillouin scattering, consisting of the generation of an intense hypersonic elastic wave and scattered light by means of an intense incoming light beam, has been found to be accompanied by damage in transparent crystals.[4.2/] Such

Brillouin scattering is characterized by a threshold light or laser power above which the effect occurs. The threshold for the effect in the case in which the radiation is not trapped in a cavity may be presumed to apply to the case of a reasonable size piece of glass irradiated by a laser beam as in the damage threshold experiments described in this report. This threshold is given by Chiao, Townes and Stoicheff[4.2/] as

$$\frac{E_o^2}{8\pi} \geq \frac{2\epsilon B}{\rho \frac{d\epsilon}{d\rho}^2 k_s k_{-1}} \left(L_s^{-1} + L_{-1}^{-1} \right)^2 \tag{45}$$

Here ϵ is the dielectric constant of the medium, B the bulk modulus, ρ the density, k_s and k_{-1} the wave vector magnitudes of the hypersonic wave and scattered light wave, respectively, and L_s and L_{-1} are the inverse absorption coefficients for the hypersonic wave and scattered light wave. Note that the threshold depends strongly on $\rho \, d\epsilon/d\rho$, or the electrostriction constant; this will appear of importance in later arguments about the damage threshold; see also Fig2. (21) and (22). Chiao, Townes, and Stoicheff's estimate of the threshold for stimulated Brillouin scattering for $L_s = 10^{-2}$cm and $L_{-1} = 10^2$cm is about 10^{10}W/cm^2 in a typical solid. Power levels obtained in the damage threshold measurements in Corning Code 0580 laser glass, for example, are of the order of 10^8-10^9W/cm^2, suggesting that it may be possible that stimulated Brillouin scattering acts as the intrinsic damage mechanism in glasses with negligable optical absorption. If such

is the case, the threshold condition for damage would naturally
depend on the various electrostriction constants in glasses under
study, and an estimate of their relative values would be very
useful. Finally, it should be noted that the absolute magnitude
of the threshold in Eq. (45) is dependent on the square of the
absorption coefficient for elastic waves at gigaherz frequencies
(as $L_s^{-1} >> L_{-1}^{-1}$) which is not well known and may lead to errors in
numerical estimates of thresholds.

4.3 Experimental Results

4.3.1 Apparatus

In order to experimentally investigate these ideas,
the same apparatus was set up as was used to investigate the case
of the absorbing media (see Fig. 2.6). The detailed description
of this apparatus is found in Section 2.3.3. Measurements were
made in glasses which did not show an appreciable absorption at
1.06μ; in general, absorptions of 3% were measurable in a one-inch
sample, so the optical absorption coefficient $\alpha \leq .01$ cm^{-1} in the
samples of glass designated "non-absorbing" and treated here.
The exception to this was arsenic trisulfide, in which
$\alpha = .10$cm^{-1} at 1.06μ; this will be discussed under the section
on dependence on index of refraction.

4.3.2 Observed Frequency Components

First of all, it has been pointed out before,
in Section 2.3.3, that there is a pronounced shift in frequency
components observed in the absorbing glasses as the absorption

is increased (see Figs. 2.7 and 2.8). In Fig. 2.7 is shown the

typical transducer signal obtained in a glass, 843KS', with

no measurable absorption ($\alpha \leq$ .01cm^{-1}). Note the high-frequency

component and high acoustical damping. As the optical absorption

is gradually increased in this glass by the addition of traces

of nickel oxide, one sees more and more low-frequency acoustic

components until at a value of α = .38cm^{-1}, one sees a trace

(Fig. 2.8) with low-frequency components consisting of the ringing

frequency of the glass block with very little damping. The

sweep speeds in Figs. 2.7 and 2.8 are 100μsec/cm; the upper traces

are integrated laser beam energy, and the lower traces are

acoustic signal from the transducer. The vertical scales in

these two photos are not the same; the ratio of acoustic pressure

amplitude to light energy P/E is about 25 times bigger in Fig. 2.8

(high optical absorption) than Fig. 2.7 (low optical absorption).

We thus see that one of the predictions of the theory, the presence

of high-frequency components in the acoustic wave, is verified.

4.3.3 The Acoustic Pressure Amplitude As A Function
of the Laser Beam Energy

Another prediction of the theory, the linearity

of acoustic pressure amplitude with integrated light energy, has

been investigated in several non-absorbing glasses. Two examples

of the results of such investigations are shown in Figs. 4.1 and

4.2 where the acoustic pressure amplitude is plotted against

integrated light energy. In Fig. 4.1 the ultrasonic oscillation

amplitude P is shown versus relative light energy on a log-log
plot for a one-inch cube of fused silica. The slope of the
line is unity, denoting P∝E; the light energy referred to is
obtained, as in the investigations on absorbing glasses, in
single Q-switched pulses of light. Various values of integrated
energy are obtained by inserting Corning glass filters with
different absorptions in the laser beam ahead of the silica cube.
The proportionality between P and E for fused silica is found
to be P = AE, where A = .70dynes/joule; this has not been corrected
for the reflection of acoustic waves at the silica-transducer
interface.

A similar plot of the acoustic pressure amplitude
versus integrated light energy, but on a linear scale, is shown
for glass 8363 in Fig. 4.2. Code 8363 is a high-lead-content
glass of index 1.98 and therefore should yield a much greater
slope of P vs E than fused silica, where the index of refraction
is 1.46, as the value of γ/n in Eq. (44) is much larger. The
observed value of A in P=AE is A=2.65dynes/joule; this has not
been corrected for reflected waves at the glass-transducer
boundary.

4.3.4   Uniform Volume Generation of Elastic Waves

An assumption of the theory, the uniform genera-
tion of elastic waves in the volume of the medium (rather than,
for example a surface effect taking place), was investigated by
preparing several samples of one glass (Corning Code 8362) in

different size cubes. Code 8362 is a lead-containing glass
with an index of refraction of 1.60, chosen because of its high
index resulting in large acoustic output, and absence of absorption
at 1.06μ. The relationship of cube size to transducer voltage
per unit light energy may be easily derived from Eq. (44).
Disregarding the factors multiplying $E = \int I dt$, we have in one
cube, say number one,

$$P_1 = BE_1. \tag{46}$$

Integrating the force over the surface of the
cylindrical volume containing the laser beam,

$$2\pi r \, \ell_1 \, P_1 = 2\pi r \, \ell_1 \, BE_1, \tag{47}$$

where ℓ_1 is the cube edge and r the laser beam radius. Assuming
that the elastic wave is not absorbed by the glass, we have

$$2\pi r \, \ell_1 P_1 \cong 4 \ell_1^2 \, P_1', \tag{48}$$

where now P_1' is measured at the surface of the cube. The
transducer responds to a total force $P_1' \, \ell_1^2$, by generating a
voltage V_1, so that

$$V_1 = D \, P_1' \, \ell_1^2, \tag{49}$$

or,

$$\frac{V_1}{E_1} = D \ell_1^2 \, \frac{P_1'}{E_1}. \tag{50}$$

Making use of (48) and (46) one has from (49) for the transducer
voltage per unit light energy in a cube of side ℓ_1,

$$\frac{V_1}{E_1} = \frac{\pi r}{2} \, BD \, \ell_1. \tag{51}$$

Similarly, in a cube of side ι_2 of the same glass, we have

$$\frac{V_2}{E_2} = \frac{\pi r}{2} BD \iota_2, \tag{52}$$

so that $V_1/E_1 : V_2/E_2 = \iota_1/\iota_2$.

The proportionality between cube edge and transducer voltage experimentally obtained is shown in Fig. 4.3. In Fig. 4.3 are plotted the values of P/E obtained from several cubes of Code 8362 glass. Each data point represents the average of six to ten single pulse laser shots. The data shows quite clearly that the elastic waves are generated uniformally in the volume of the glass.

4.3.5 Dependence of the Generation of Elastic Waves on Index of Refraction

The one remaining feature of Eq. (44) which requires investigation is the dependence of the induced elastic wave pressure on index of refraction. Accordingly, a number of different glasses of various compositions ranging in index of refraction from 1.46 (fused silica) to arsenic trisulfide, index 2.47, have been prepared as cut and polished cubes. The velocity for longitudinal waves of each glass in this series was measured, using pulse techniques at 3.43MHZ, and the cubes cut in corresponding sizes so as not to be frequency sensitive near 266KHZ, the ringing frequency of the transducer. The values of P/E for each glass were then determined in 6 to 10 single-pulse shots of the Q-spoiled laser, typical probable errors in the results being

3% to 5%. The results of these data runs were all scaled up to a one-inch maximum cube size using Eq. (46) and (47), and the results plotted against index of refraction, see Fig. 4.4. In Fig. 4.4 are plotted the values of P/E obtained, multiplied by an arbitrary scale factor, against index of refraction for 10 glasses. The solid curve is a plot of $\frac{(n^2-1)(n^2+2)}{n}$, which is obtained from Eq. (44) for the index dependence. The solid curve is forced arbitrarily to pass through the experimental value for Code 8363 glass at n = 1.98, and the remainder of the curve is calculated and plotted as shown. Absolute values of the ordinate scale can be obtained by multiplying the scale shown by .156 dynes/joule. These values of P/E for specific glasses are not corrected for the reflection of the elastic wave at the glass-transducer boundary. The fit in any case is quite good, considering the approximations involved in deriving Eq. (22) from the Clausius-Mosotti relation in a number of glass-forming systems. These systems range from fused silica to lanthanum-borate (890ACY) through lead-containing glasses (8362 and 8363) to arsenic trisulfide. It was felt justified to include arsenic trisulfide in this index-of-refraction data, even though it had a measurable optical absorption at 1.06μ ($\alpha=.10cm^{-1}$), because the character of the acoustic pulses at the transducer was observed to be characteristic of a non-absorbing glass (high-frequency components predominating). The fact that there was small absorption may account for the fact that arsenic trisulfide lies

rather high on the index curve, above the "theory" line, as a portion of the observed signal may be absorptive in character. The experimental points obtained in Fig. 4.4 may be regarded as experimentally determined relative values of $\rho \frac{d\epsilon}{d\rho}$, which coefficient enters into the equation for stimulated Brillouin scattering Eq. (45). One therefore sees that, <u>other things being equal</u>, glasses far down on the curve of Fig. 4.4 should be more resistant to damage than those up high, such as arsenic tri-sulfide. For example, fused silica should be quite resistant to damage in high-intensity laser beams. High damage thresholds for fused silica in comparison with other glasses have been reported[4.3/], although this is not conclusive evidence of the connection between damage threshold and low acoustic output as there are other parameters in Eq. (45) unaccounted for.

4.3.6 Laser Bandwidth

The generation of elastic waves in nonabsorbing media may be expected to be independent of frequency in the low frequency limit, as has been pointed out. However, the upper frequency limit may be expected to depend on the bandwidth of the Q-switched laser used in the experimental work, as of course, no acoustic frequencies are generated which are not present as differences in the laser beam. Thus one may predict the generation of phonons by the laser beam up to a cutoff frequency of about 4ϵ, where 2ϵ is the gaussian halfwidth of the laser beam intensity vs. frequency curve.

The first work on the bleachable dye Q-switch for
the neodymium glass laser[4.4] has been followed by research concerned
with time-resolved pulse structure and the obtained bandwidth.[4.5-4.8]
The bandwidth of bleachable dye Q-switched pulses from neodymium
glass lasers has been reported by McFarland and co-workers[4.5] to
be very narrow, their reported value being .02Å. In contradiction
with this, DeMaria et al[4.6-4.8] report bandwidths with this type
of experimental setup to be very broad, from 40Å[4.7] to 180Å[4.8]. The
apparent difference between McFarland's and DeMaria's results can
be explained on the basis that McFarland prepared a polymethine
dye for use in his Q-switch, while DeMaria used a different dye[*]
which is marketed under the name Eastman Q-Switch Solution #9740.
In the case of a bleachable dye Q-switched ruby laser, one obtains
a marked narrowing of the bandwidth in going from the non-Q-switched
to the Q-switched case.[4.10-4.11] With the non-Q-switched neodymium
glass laser, bandwidths of 50Å to 100Å are common.[4.9] Since
DeMaria reports the same sort of bandwidths for the bleachable
dye Q-switched glass laser, there appears to be no narrowing of
the bandwidth by means of the use of Eastman #9740 Q-Switch
Solution over the non-Q-switched case, as has occurred with the
ruby laser. Quoted figures of the bandwidth in the literature
have not been tied to energy output or dye density, nor have line

---

[*]Private communication, Eastman Organic Chemicals Division

halfwidths been given. A need, therefore, exists for further work
on the bandwidth of the neodymium glass laser.

A diagram of the experimental arrangement is shown
in Fig. 4.5. The usual arrangement of mirrors, Q-switch cell and
laser rod is set up to produce giant pulses of .1-.5 joule total
energy exiting from the output, or 85% reflectance mirror. The
mirrors are dielectric-coated glass flats. The laser rod is a
cylinder 15cm long x 1.5cm diam. Corning Nd glass, Code 0580;
the ends are polished flat and parallel. The Q-switch cell con-
sists of a pair of fused silica flats separated by a spacer and
clamped so as to produce a path length in the Q-switch solution
of 1.7mm; the Q-switch solution is Eastman Kodak #9740 dye in
chlorobenzene solution.

The laser beam which exits from the output mirror
is split by a 45% reflectance dielectric mirror and one part of
the beam enters a ½ meter Bausch & Lomb grating spectrometer
through a set of filters which attenuate the beam to produce the
desired exposure in the camera. The camera photographs the smeared
spectrum imaged at the spectrometer output on a ground glass
screen to which a scale has been cemented. Eastman Kodak Type 1-Z
infrared plates are used in the camera, and developed in Eastman
D-19 developer diluted so as to reduce undesirable fog in the plates.

The other portion of the beam passes through the
45% mirror and onto a ground glass diffusing screen-attenuating
filter combination to eliminate the effects of the filamentary

nature of the laser beam and to produce levels at the photodiode which will not damage the instrument (an Edgerton, Germeshausen and Grier Lite-Mike Model 561). The output of the Lite-Mike is displayed in an integrated energy mode and photographed on the oscilloscope. The photodiode is calibrated by substituting a calorimeter for the grating spectrometer.

The grating, in use, produces a smearing of the spectrum at the image plane of the spectrometer plus the breadth of the entrance slit. The optics of this system have been checked by allowing the beam of a He-Ne laser to enter the system and photographing the resulting spread at the exit. Therefore, a series of photographs have been made of the laser spread at a Q-switch cell absorbance of .35 (transmittance 45%) and .25 (transmittance 56%) as a function of energy output. A typical raw-data run is shown in Fig. 4.6. Here the total bandwidth B down to fog level in the plate has been measured by microscopically examining Type 1-Z plates exposed and developed from single-pulse laser outputs. The output energy E_o is given in joules; this varies from shot to shot and is not repeatable, a series being taken to produce the data. Since increased exposure of the plate would produce the appearance of increased bandwidth without its necessarily being any greater, another series of exposures were taken to produce another raw data curve similar to Fig. 4.6, but with a different exposure due to a different filter set being used on the spectrometer entrance slit. Assuming that the

intensity versus frequency curve of the laser is gaussian, we have for one data point with one filter set #1,

$$I_1 = \frac{.48}{\sqrt{\pi}\ \epsilon}\ e^{\dfrac{-.23(f_1-f_o)^2}{\epsilon^2}}, \tag{53}$$

where f_o is the laser center frequency and 2ϵ the gaussian halfwidth.

For the other filter set #2 we have similarly

$$I_2 = \frac{.48}{\sqrt{\pi}\ \epsilon}\ e^{\dfrac{-.23\ (f_2-f_o)^2}{\epsilon^2}}, \tag{54}$$

Taking the ratio we have

$$I_1/I_2 = e^{\dfrac{-.23}{\epsilon^2}}\ [(f_1-f_o)^2 - (f_2-f_o)^2]. \tag{55}$$

and since I_1/I_2 is known equal to the ratio of the filter factors at the same laser energy, 2ϵ, the gaussian halfwidth, may be calculated from two bandwidth vs energy curves with different filter factors. The gaussian halfwidths so calculated at convenient intervals over a range of energies E_o for two different dye absorbances are shown in Fig. 4.7. The pump energy for these Q-switch absorbances was 4,700 joules for the .25 case and 7,200 joules for the .35 case. It can be seen from the curves that much larger halfwidths are obtained than with the case of the bleachable dye Q-switched ruby laser,[4.10,4.11]/and that the bandwidth increases rapidly with the energy output. The bandwidth also increases somewhat with dye density, but this also results in greater energy output.

The non-Q-switched bandwidth has also been
investigated for this particular laser by reading directly the
width of the wavelength spread on the plates exposed in the
system of Fig. 4.5, with the Q-switch removed. The center wave-
length appeared at $10,615 \pm 15$Å. The total bandwidth B vs. energy
output E_o is shown in Fig. 4.8. Fig. 4.8 shows the sort of thing
that would be expected from previous data on the spectral output
of a Nd-glass laser.[4.9/] When bandwidth data in the non-Q-switched
case, which is not gaussian, is analyzed in the gaussian manner
as in the Q-switched case, it yields an ϵ vs E_o curve which rises
rapidly, then levels off. This can be understood by observing
the character of the resolved line spectra;[4.9/] at first as E_o
increases, the effect is to greatly broaden the output. Later,
as E_o increases, a large number of lines near the laser frequency
are excited, thus resulting in a levelling off of the calculated
halfwidth.

The laser pump energies for the specific bandwidths
may be inferred from Fig. 4.9, where the energy output E_o is plotted
vs the pump or energy input E_i. The threshold E_t for this particular
laser is seen to be approximately 1700 joules, so that levels in
relation to threshold can be found.

In conclusion, the Q-switched and non-Q-switched
data show that phonon frequencies $\frac{\Omega}{2\pi} \sim 10^{12}$ herz may be generated
by the passage of a Nd-glass laser beam through transparent media,
with the upper limit increasing with laser beam energy (and

Q-switch dye density, in the Q-switched case). On comparing the bandwidths for the non-Q-switched and Q-switched case, one sees that Q-switching tends to broaden the bandwidth with the use of this dye rather than narrow it; of course, the energies are not comparable in the two cases. Insertion of the Q-switch reduced the energy output in single pulses to .6-1.5% of the non-Q-switched value.
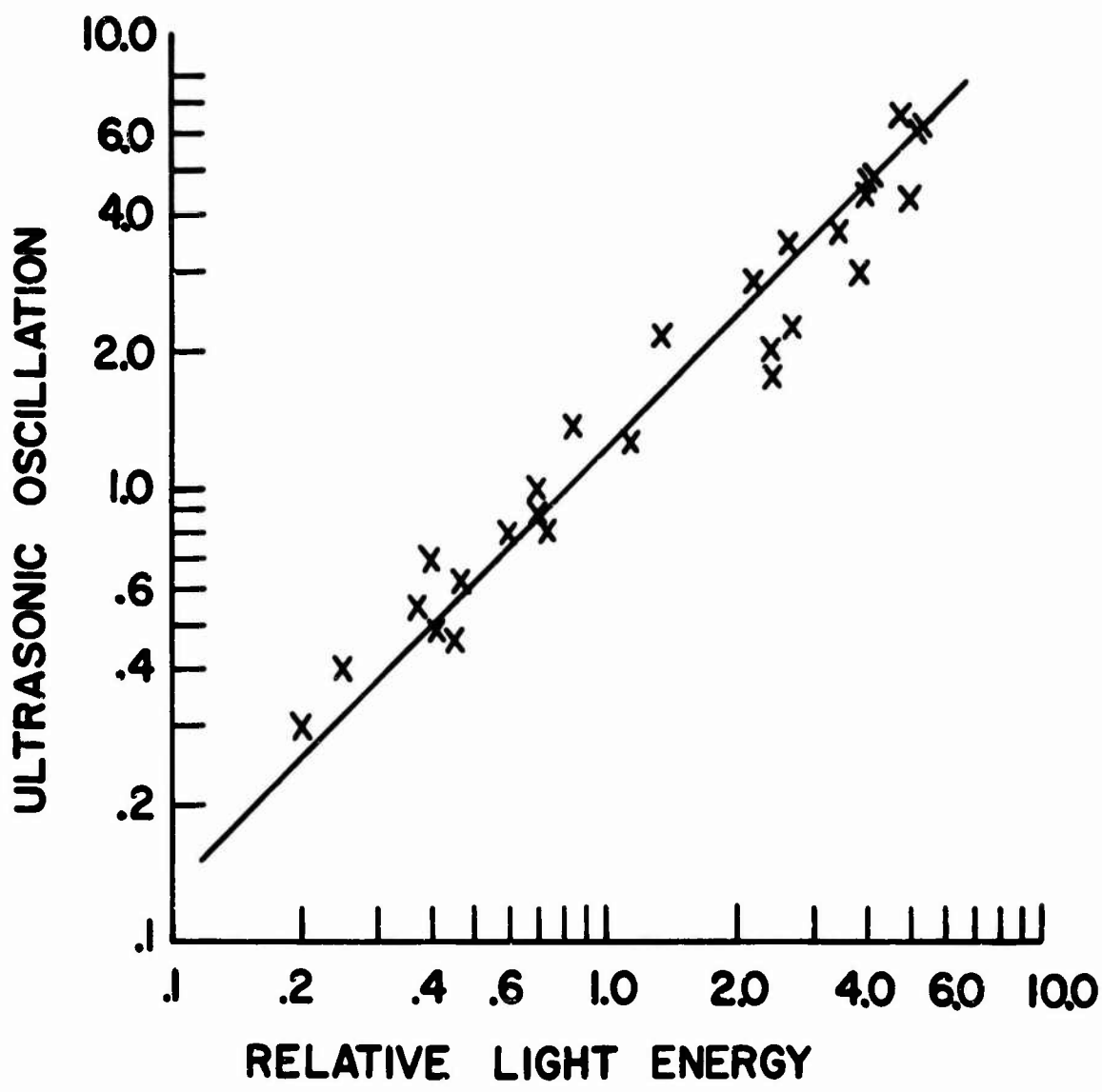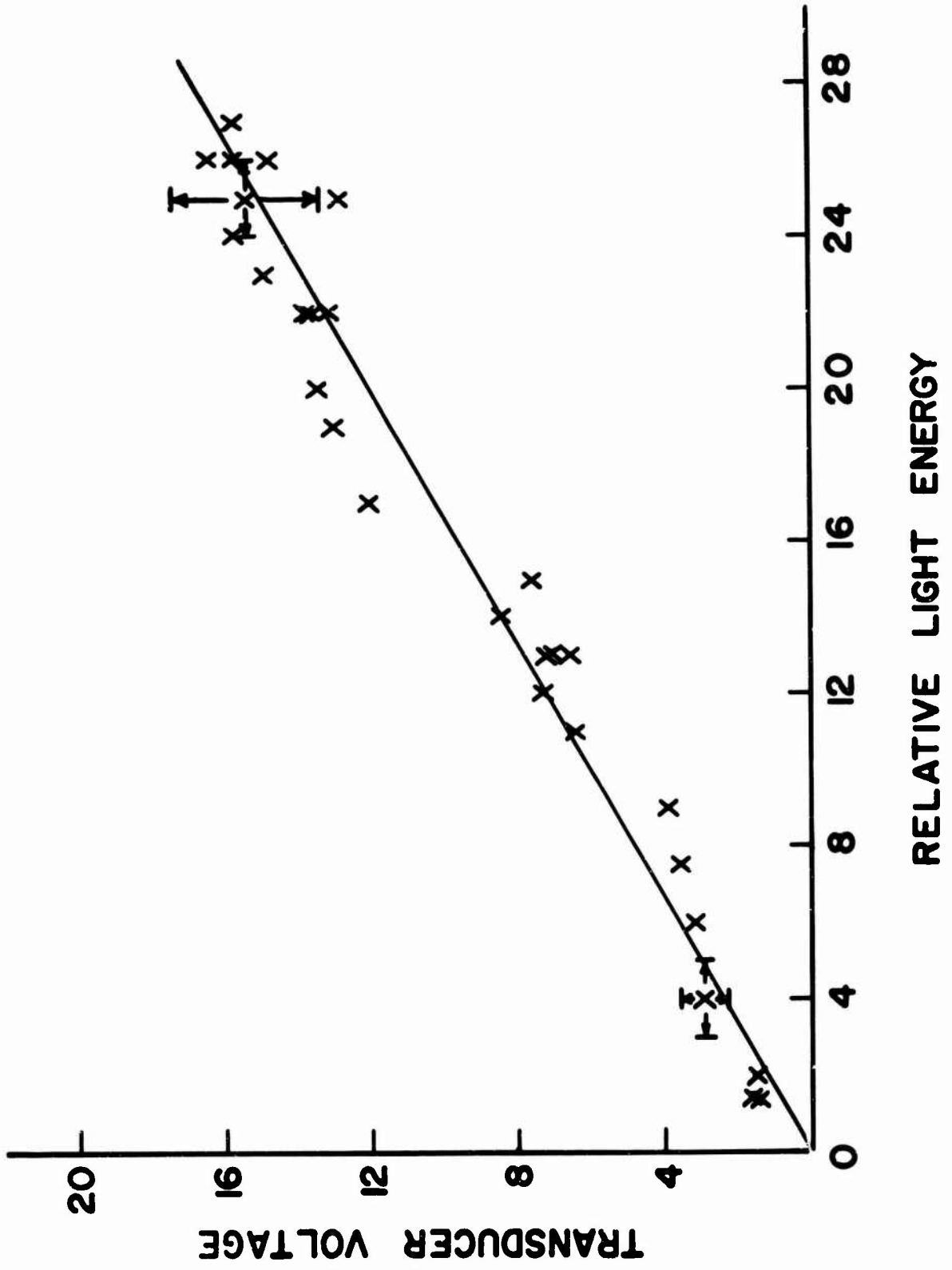
Fig. 4.1   Relative Induced Elastic-pulse Pressure Amplitude
Versus Relative $E = \int I\,dt$ for fused silica.

Fig. 4.2 Relative Induced Elastic Pulse Pressure Amplitude Versus Relative $E = \int I\,dt$ for Code 8363 Glass.
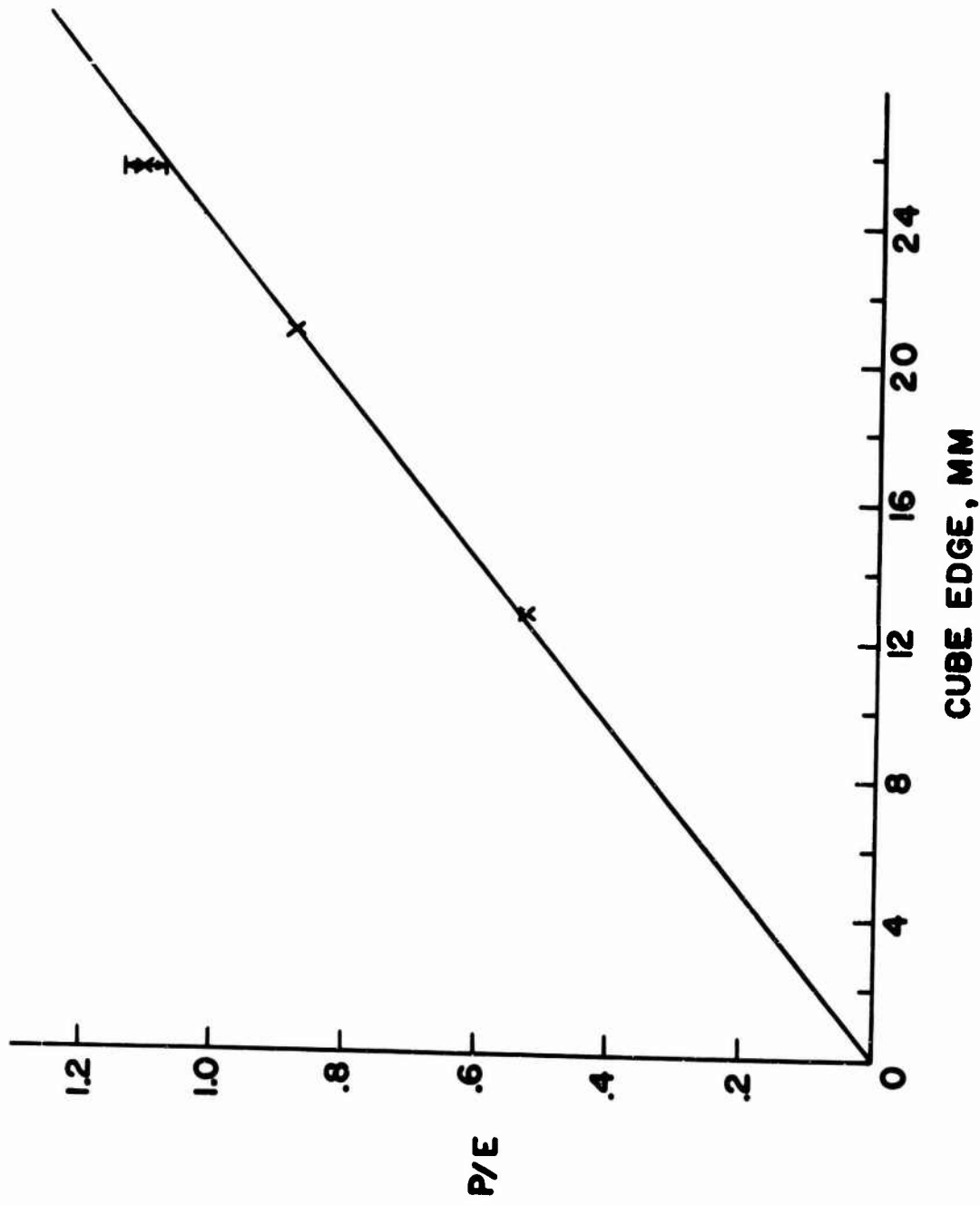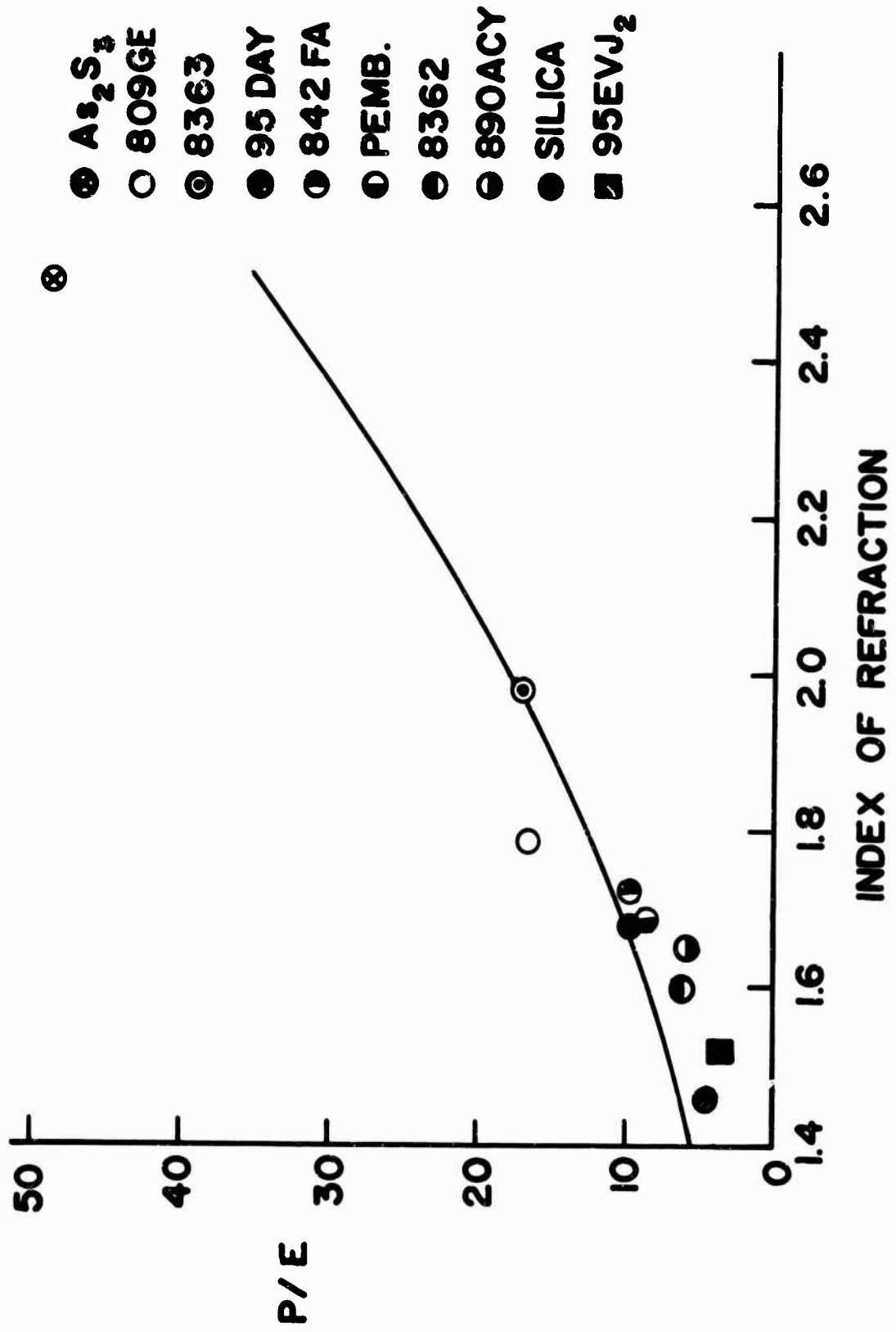
Fig. 4.3   Relative Induced Transducer Voltage Per Unit Light Energy
Versus Cube Size in Cubes of Code 8362 Glass.

Fig. 4.4 Relative Induced Elastic Pulse Pressure Amplitude Per Unit Relative Light Energy Versus Index of Refraction in Various Glasses.
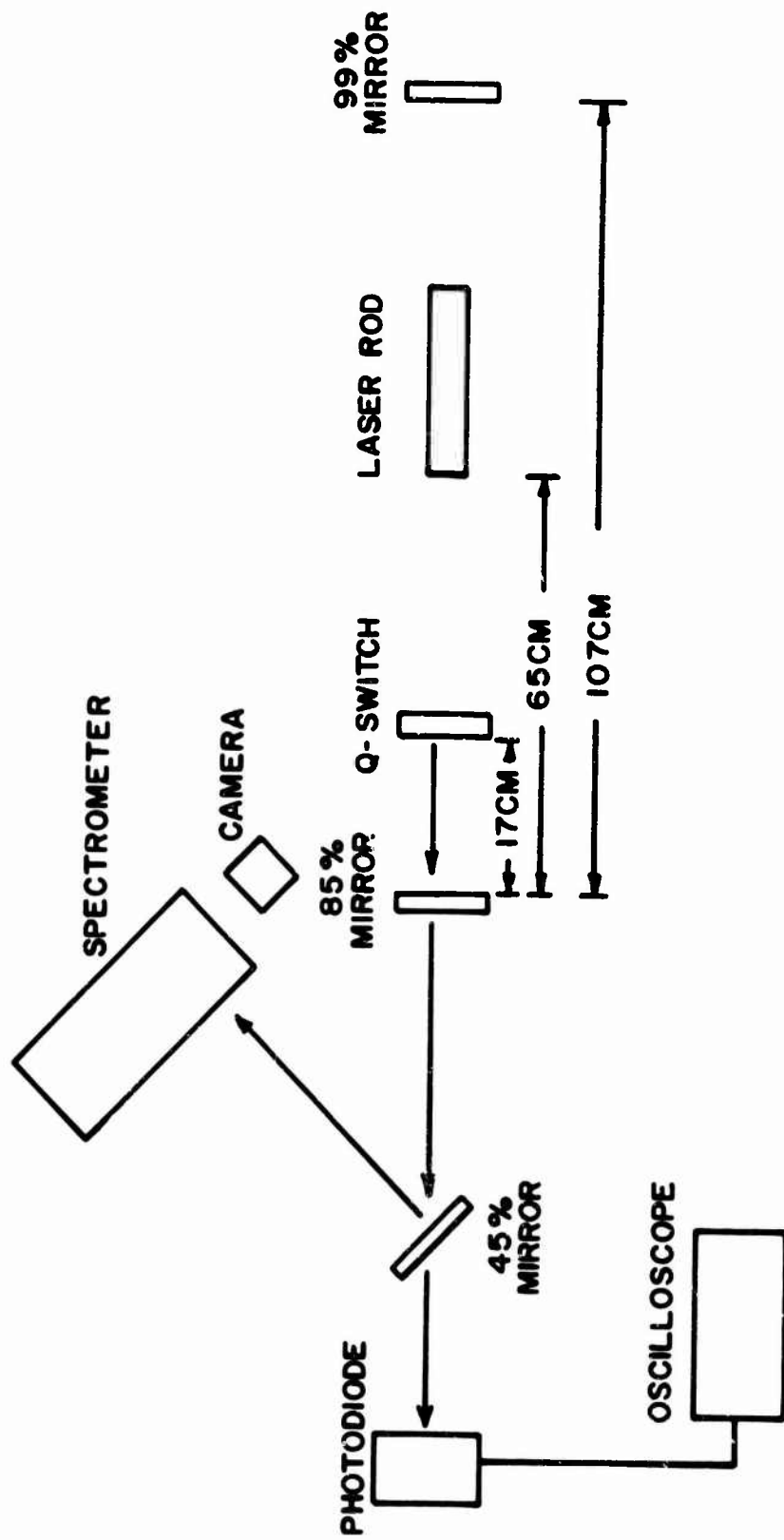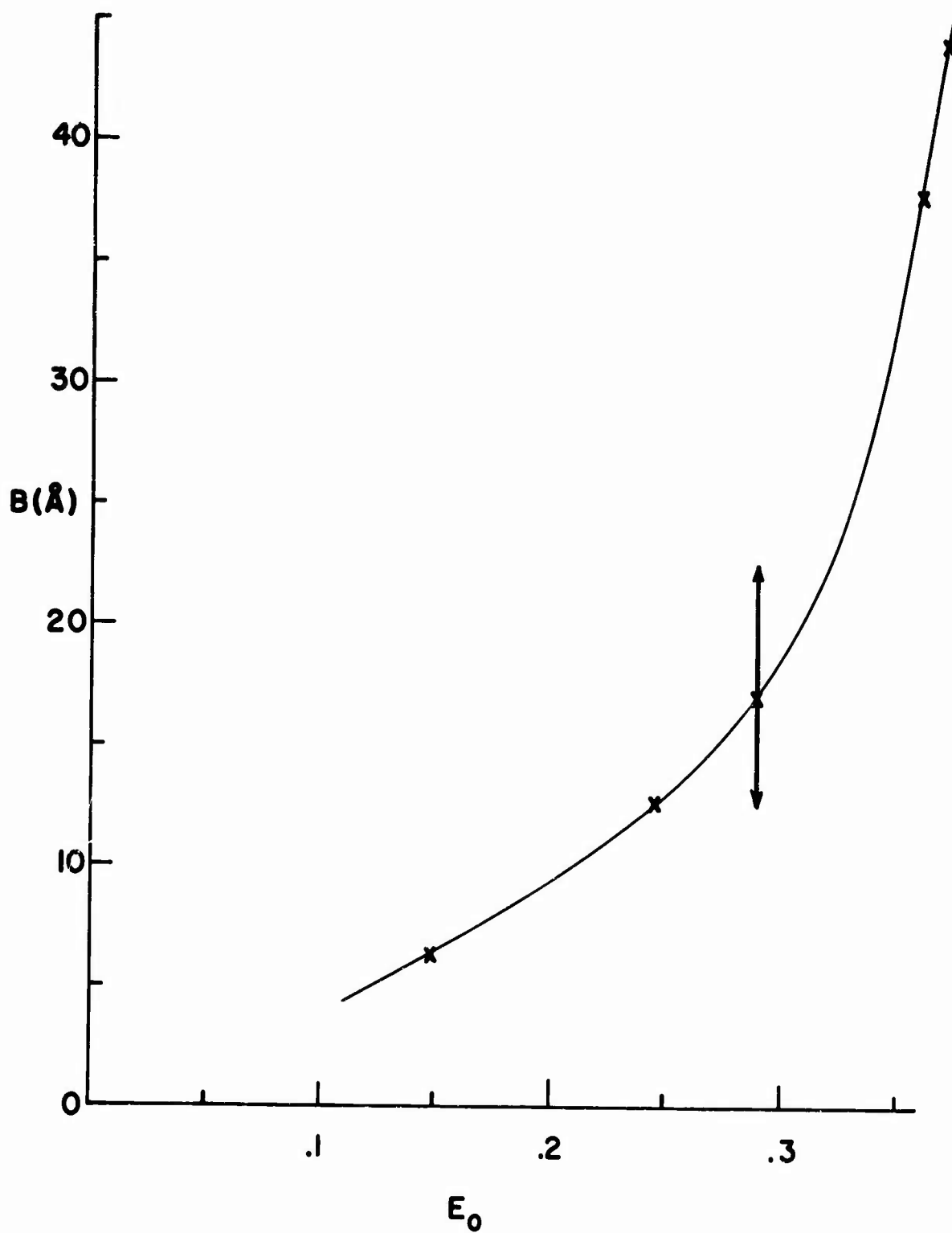
Fig. 4.5 Experimental Apparatus

Fig. 4.6 Q-switched Spread B, in Angstroms, Versus Output
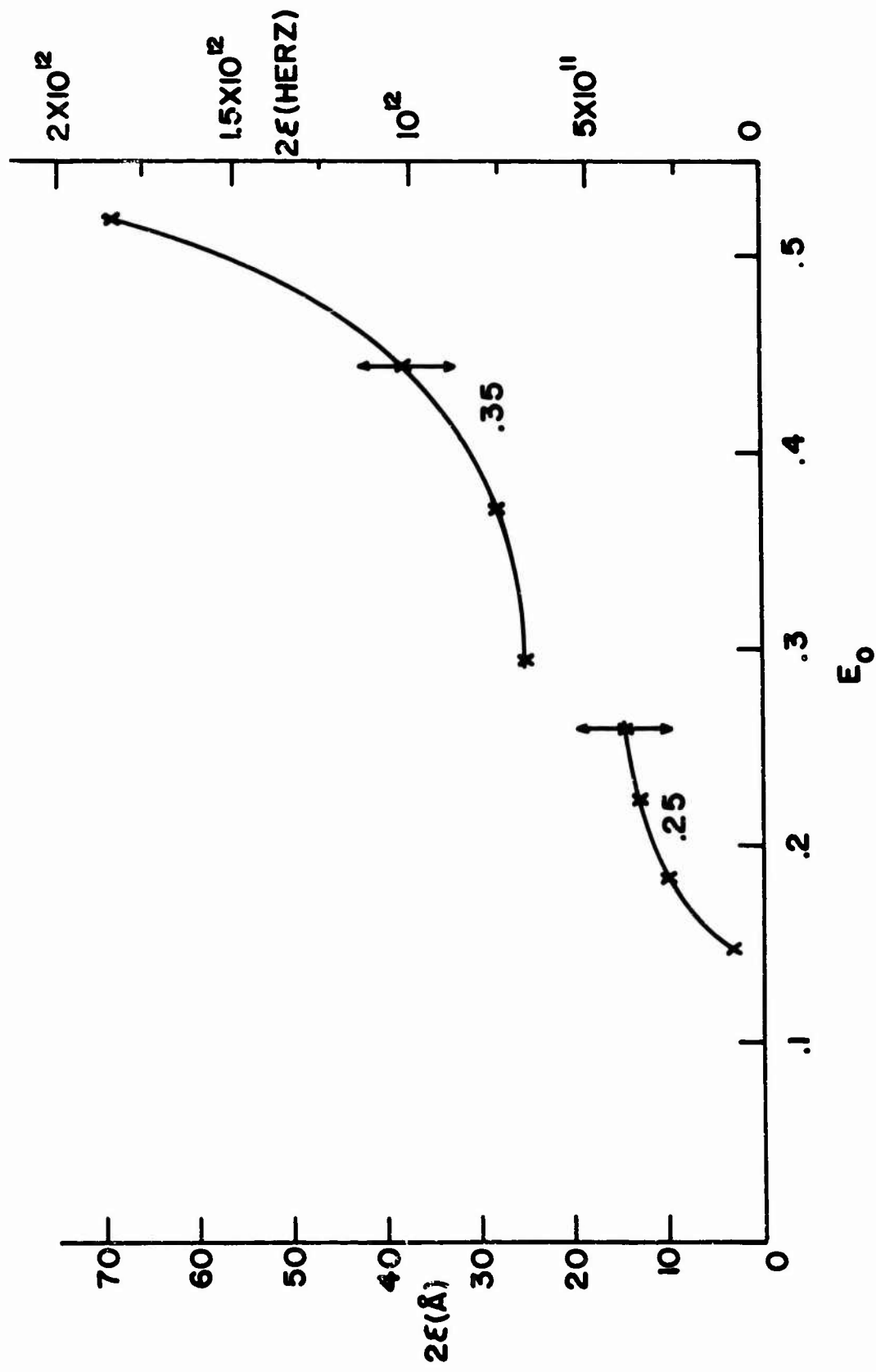Energy E_o, in Joules, at a Dye Absorbance of .25.

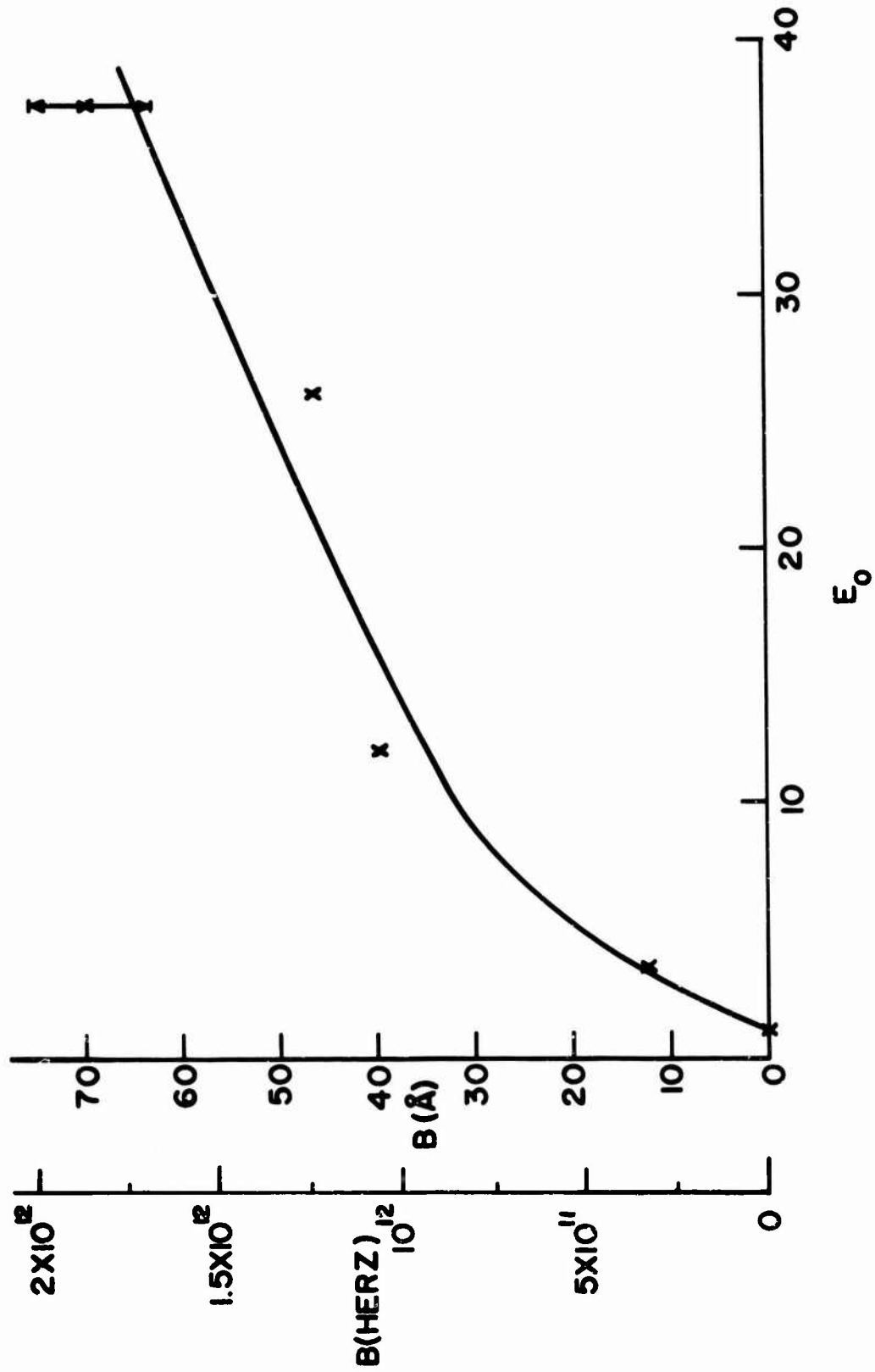Fig. 4.7 Gaussian Bandwidths 2ϵ versus Energy Output E_o, in Joules, for Dye Absorbances of .25 and .35.

Fig. 4.8 Non Q-switched Frequency (wavelength) Spread B
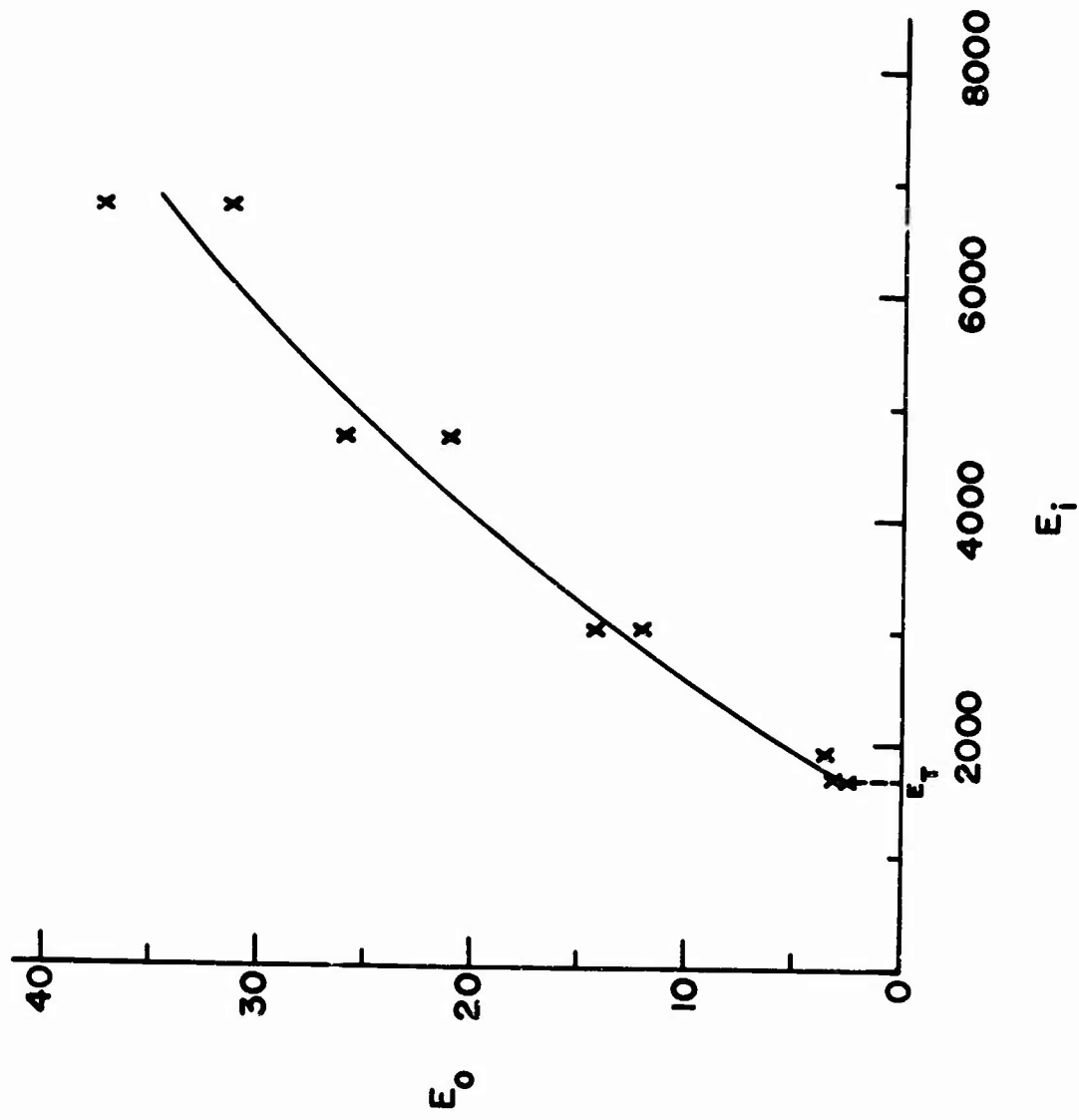Versus Energy Output E_o, in Joules.

Fig. 4.9 Non Q-switched Energy Output E_o Versus Energy Input E_i, in Joules.

REFERENCES

1.1   Miller, R. A. and N. F. Borrelli, Appl. Optics $\underline{6}$, 164 (1967)

2.1   Maurer, R. D. et al., "Glass Laser Damage Research",
      Semiannual Report under Contract N00014-66-C0159, June, 1966.

2.2   Miller, R. A. and N. F. Borrelli, Applied Optics $\underline{6}$, 164 (1967).

2.3   Redwood, M., J. Acoust. Soc. Am. $\underline{33}$, 527 (1961).

3.1   Maurer, R. D. et al, "Glass Laser Damage Research",
      Semiannual Report under Contract N00014-66-C0159, June, 1966.

3.2   S. Sirgh and J. Geusic, Phys. Rev. Letters $\underline{17}$, 865 (1966).

3.3   K. Hauptmanova, J. Pantoflicek and K. Patek, Phys. Stat.
      Sol. $\underline{9}$, 525 (1965).

3.4   T. C. MacAvoy, et al., "Glass Laser Research", Annual
      Report under Contract No. Nonr-3833(00), Project Code No.7300,
      Order No. 306-62, AD-419196, Corning Glass Works (June, 1963).

3.5   G. H. Dieke and B. Pandey, in Proceedings of the Symposium
      on Optical Masers (Polytechnic Press, New York, 1963), p. 327.

3.6   R. D. Maurer, et al., "Glass Laser Research", Semiannual
      Report under Contract No. Nonr-3833(00), Project Code No. 7300,
      Order No. 306-62, AD612964, Corning Glass Works (January, 1965).

3.7   A. Cabezas and R. Treat, J.A.P. $\underline{37}$, 3556 (1966).

3.8   G. Birnbaum, Optical Masers (Academic Press, New York, 1964) p.21.

4.1   M. A. Kastler, Compt. Rend. $\underline{259}$, 4535-4540 (1964).

4.2   R. Y. Chiao, C. H. Townes, and B. P. Stoicheff, Phys. Rev.
      Letters $\underline{12}$, 592-595 (1964).

4.3   Research on Properties of Laser Devices, Eighth Quarterly
      Summary Technical Report AF 49(638)-673.

REFERENCES CONT'D

4.4   B. H. Soffer and R. H. Hoskins, Nature <u>204</u>, 276 (1964).

4.5   B. B. McFarland, R. H. Hoskins, and B. H. Soffer, Nature <u>207</u>, 1180-1181 (1965).

4.6   A. J. DeMaria, D. A. Stetser, and H. Heynau, Appl. Phys. Letters <u>8</u>, 174-176 (1966).

4.7   A. J. DeMaria, D. A. Stetser, and H. Heynau, Digest of Technical Papers, 1966 International Quantum Electronics Conference, Paper 4A-7, Page xxiii.

4.8   D. A. Stetser and A. J. DeMaria, Appl. Phys. Letters <u>9</u>, 118-120 (1966).

4.9   P. A. Miles, Quoted by R. D. Maurer in <u>Proceedings of the Symposium on Optical Masers,</u> Polytechnic Press, Polytechnic Institute of Brooklyn, New York - 1963 (pp. 445-446).

4.10 B. H. Soffer, J. Appl. Phys. <u>35</u>, 2551 (1964).

4.11 M. Hercher, Appl. Phys. Letters <u>7</u>, 39-41 (1965).

DOCUMENT CONTROL DATA - R&D

(Security classification of title, body of abstract and indexing annotation must be entered when the overall report is classified)

1 ORIGINATING ACTIVITY *(Corporate author)*	2a. REPORT SECURITY CLASSIFICATION
Corning Glass Works Corning, New York 14830	Unclassified
	2b GROUP NA

3. REPORT TITLE

Glass Laser Damage Research

4. DESCRIPTIVE NOTES *(Type of report and inclusive dates)*

Final Technical Report

5. AUTHOR(S) *(Last name, first name, initial)*

Maurer, R. D.   Lester, W. W.   Vance, M. E.

6. REPORT DATE	7a. TOTAL NO. OF PAGES	7b. NO. OF REFS
June 1967	65	23

8a. CONTRACT OR GRANT NO.	9a. ORIGINATOR'S REPORT NUMBER(S)
N00014-66-C0159	NA
b. PROJECT NO. 7300	
c.	9b. OTHER REPORT NO(S) *(Any other numbers that may be assigned this report)* NA
d.	

10. AVAILABILITY/LIMITATION NOTICES

Qualified requestors may obtain copies of this report from DDC

11. SUPPLEMENTARY NOTES	12. SPONSORING MILITARY ACTIVITY
NA	Office of Naval Research

13. ABSTRACT This report covers an experimental investigation into the damage of glass by high intensity, 1.06u wavelength light pulses of millisecond duration. Damage due to optical absorption by impurities is demonstrated by ease of damage, above some intrinsic level, proportional to the measured optical absorption. An additional source of damage is optical absorption at 1.06u from the excited (fluorescing) state of the neodymium ion. Evidence for this mechanism is presented, and an approximate value of the excited state absorption cross section determined. The nonradiative decay (heating) back to the initial excited state is assumed to be the source of damage, and this appears reasonable from other data.

Studies of opto-acoustic coupling are presented and their connection with stimulated Brillouin scattering denoted. Measured coupling constants for different glasses, which are shown to be devoid of impurity optical absorption effects are presented. Stimulated Brillouin scattering as a cause of damage suggests correlation between these opto acoustic coupling constants and damage thresholds. Initial qualitative agreement between the two is encouraging enough to warrant further investigation of this technique as a way of predicting damage thresholds.

DD FORM 1473
1 JAN 64

14. KEY WORDS	LINK A		LINK B		LINK C	
	ROLE	WT	ROLE	W T	ROLE	WT
laser effects, glass lasers, damage by laser light						

INSTRUCTIONS

1. **ORIGINATING ACTIVITY:** Enter the name and address of the contractor, subcontractor, grantee, Department of Defense activity or other organization (*corporate author*) issuing the report.

2a. **REPORT SECURITY CLASSIFICATION:** Enter the overall security classification of the report. Indicate whether "Restricted Data" is included. Marking is to be in accordance with appropriate security regulations.

2b. **GROUP:** Automatic downgrading is specified in DoD Directive 5200.10 and Armed Forces Industrial Manual. Enter the group number. Also, when applicable, show that optional markings have been used for Group 3 and Group 4 as authorized.

3. **REPORT TITLE:** Enter the complete report title in all capital letters. Titles in all cases should be unclassified. If n meaningful title cannot be selected without classification, show title classification in all capitals in parenthesis immediately following the title.

4. **DESCRIPTIVE NOTES:** If appropriate, enter the type of report, e.g., interim, progress, summary, annual, or final. Give the inclusive dates when a specific reporting period is covered.

5. **AUTHOR(S):** Enter the name(s) of author(s) as shown on or in the report. Enter last name, first name, middle initial. If military, show rank and branch of service. The name of the principal author is an absolute minimum requirement.

6. **REPORT DATE:** Enter the date of the report as day, month, year; or month, year. If more than one date appears on the report, use date of publication.

7a. **TOTAL NUMBER OF PAGES:** The total page count should follow normal pagination procedures, i.e., enter the number of pages containing information.

7b. **NUMBER OF REFERENCES:** Enter the total number of references cited in the report.

8a. **CONTRACT OR GRANT NUMBER:** If appropriate, enter the applicable number of the contract or grant under which the report was written.

8b, 8c, & 8d. **PROJECT NUMBER:** Enter the appropriate military department identification, such as project number, subproject number, system numbers, task number, etc.

9a. **ORIGINATOR'S REPORT NUMBER(S):** Enter the official report number by which the document will be identified and controlled by the originating activity. This number must be unique to this report.

9b. **OTHER REPORT NUMBER(S):** If the report has been assigned any other report numbers (*either by the originator or by the sponsor*), also enter this number(s).

10. **AVAILABILITY/LIMITATION NOTICES:** Enter any limitations on further dissemination of the report, other than those imposed by security classification, using standard statements such as:

  (1) "Qualified requesters may obtain copies of this report from DDC."

  (2) "Foreign announcement and dissemination of this report by DDC is not authorized."

  (3) "U. S. Government agencies may obtain copies of this report directly from DDC. Other qualified DDC users shall request through

                                                      ."

  (4) "U. S. military agencies may obtain copies of this report directly from DDC. Other qualified users shall request through

                                                      ."

  (5) "All distribution of this report is controlled. Qualified DDC users shall request through

                                                      ."

If the report has been furnished to the Office of Technical Services, Department of Commerce, for sale to the public, indicate this fact and enter the price, if known.

11. **SUPPLEMENTARY NOTES:** Use for additional explanatory notes.

12. **SPONSORING MILITARY ACTIVITY:** Enter the name of the departmental project office or laboratory sponsoring (*paying for*) the research and development. Include address.

13. **ABSTRACT:** Enter an abstract giving a brief and factual summary of the document indicative of the report, even though it may also appear elsewhere in the body of the technical report. If additional space is required, a continuation sheet shall be attached.

It is highly desirable that the abstract of classified reports be unclassified. Each paragraph of the abstract shall end with an indication of the military security classification of the information in the paragraph, represented as (TS), (S), (C), or (U).

There is no limitation on the length of the abstract. However, the suggested length is from 150 to 225 words.

14. **KEY WORDS:** Key words are technically meaningful terms or short phrases that characterize a report and may be used as index entries for cataloging the report. Key words must be selected so that no security classification is required. Identifiers, such as equipment model designation, trade name, military project code name, geographic location, may be used as key words but will be followed by an indication of technical context. The assignment of links, rules, and weights is optional